Noble gas as a proxy to understand the evolutionary path of migrated CO2 in a shallow aquifer system

Journal Pre-proof

Noble gas as a proxy to understand the evolutionary path of migrated CO_2 in a shallow aquifer system

YeoJin Ju, Seong-Sun Lee, Dugin Kaown, Kang-Kun Lee, Stuart M.V. Gilfillan, Doshik Hahm, Keyhong Park

PII: S0883-2927(20)30095-0

DOI: https://doi.org/10.1016/j.apgeochem.2020.104609

Reference: AG 104609

To appear in: *Applied Geochemistry*

Received Date: 6 October 2019

Revised Date: 18 January 2020

Accepted Date: 20 April 2020

Please cite this article as: Ju, Y., Lee, S.-S., Kaown, D., Lee, K.-K., Gilfillan, S.M.V., Hahm, D., Park, K., Noble gas as a proxy to understand the evolutionary path of migrated CO_2 in a shallow aquifer system, *Applied Geochemistry* (2020), doi: https://doi.org/10.1016/j.apgeochem.2020.104609.

Noble gas as a proxy to understand the evolutionary path of migrated CO_2 in a shallow aquifer system

YeoJin Ju[1], Seong-Sun Lee[1], Dugin Kaown[1], Kang-Kun Lee[1,*], Stuart M.V. Gilfillan[2], Doshik Hahm[3], Keyhong Park[4]

[1]School of Earth and Environmental Sciences, Seoul National University, 1 Gwanak-ro, Gwanak-gu, Seoul, 08826, South Korea.

[2]School of GeoSciences, The University of Edinburgh, Grant Institute, James Hutton Road, Edinburgh EH9 3FE, UK.

[3]Department of Oceanography, Pusan National University, Busan, South Korea.

[4]Division of Polar Ocean Science, Korea Polar Research Institute, Incheon, South Korea.

Email: jinee18@snu.ac.kr, soon3311@snu.ac.kr, dugin1@snu.ac.kr, stuart.gilfillan@ed.ac.uk, hahm@pusan.ac.kr, keyhongpark@kopri.re.kr.

*Corresponding author. Tel.: +82 2 873 3647. E-mail address: kklee@snu.ac.kr.

Abstract

To provide confidence in the safety of a carbon capture and storage (CCS) project, researchers have focused on developing monitoring techniques to trace the unlikely, but potentially possible, migration of CO_2 from a deep reservoir. Among the various techniques, noble gas tracing is a beneficial approach, owing to the unique noble gas fingerprints present in injection fluids, the deep reservoir, and the shallow aquifer above the storage area. However, the value of this approach has been limited to demonstrations in a natural analogue CO_2-rich reservoir and an artificial injection test site. Therefore, further efforts are required to link those valuable observations to an actual CCS site. In this study, we outline how to use these tracers for actual monitoring work in a shallow aquifer system. First, two artificial injection tests were performed using He, Ar, Kr, and SF_6 to understand the behavior of the leaked plume in the shallow aquifer system. In both tests, the noble gas ratio remarkably changed with the solubility-controlled process and the mixing process. To extend and link the valuable findings from the artificial injection tests to an actual CO_2 leakage event, we performed a leakage simulation using data from a real CO_2 injection site, i.e., the Weyburn–Midale site. This simulation suggested that combinations of ^{4}He with other heavier noble gases can be used to monitor CO_2 leakage, as they allow us to separate and explain the major interactions governing the migration of the leaked plume in the shallow aquifer system. Additionally, although the high CO_2 density of a dissolved plume is known to add uncertainty in quantitative approaches, the influence of those effects was negligible when compared to the errors arising from the wide variation in the noble gas fingerprints in the leaked CO_2. This study, therefore, provides insight into the evolutionary path of the migrated CO_2 plume in the shallow aquifer system and to the results can be used to inform the tracing of a leakage source within a shallow aquifer despite various mechanisms complicating the plume distribution.

Keywords: Carbon capture and storage; CO_2 leakage; noble gas tracing; degassing; inherent tracer; monitoring

1 Introduction

A carbon capture and storage (CCS) project uses an impermeable or low-permeability cap rock to trap sequestered CO_2 in a formation without leakage. The CO_2 injected into the storage formation is sequestrated by subsurface trapping mechanisms, namely structural/stratigraphic trapping, residual trapping, solubility trapping, and mineral trapping mechanisms. Evidence shows that these are effective on a geologic time scale (Alcalde and Flude et al., 2018; Altman et al., 2014; IPCC, 2005). However, a recent event where artificial injection activity of water in an enhanced geothermal system (EGS) triggered a 5.5 magnitude earthquake of in Pohang, South Korea (Lee et al., 2019) led to increased public awareness of the potential issues of injecting fluids into the subsurface in Korea. This situation led to the temporary closure of a CO_2 capture and storage demonstration project intended to be performed in the Pohang Basin, South Korea (Chen et al., 2018). Furthermore, it was alleged that CO_2 that had leaked from the storage formation at the Weyburn-Midale site had polluted a nearby shallow groundwater zone (Beaubien et al., 2013). These examples highlight the need for a robust monitoring regime of any future geological storage site to provide reassurance that CO_2 is being safely stored and that any migration from the site can be detected.

The monitoring of leaked CO_2 is often complicated by naturally occurring CO_2 in the subsurface system. The distribution of CO_2 is very heterogeneous in a natural groundwater system as a result of chemical, biological, and physical interactions (Risk et al., 2015). The use of stable C isotopes for leakage monitoring can also be challenging because their signals in leaked fluids can overlap with those of common surface sources (e.g., landfills) (Györe et al., 2017), following bacterial activity that enriches the ^{13}C by an oxidation process (Whiticar et al., 1999). However, noble gases are chemically and biologically inert, and are only affected by quantifiable physical processes in a shallow aquifer system. Therefore, noble gases can provide a means to separate and explain the physical processes in a biochemically complicated system (Kilgallon et al., 2018). The benefits of this tracer were first recognized in an

enhanced oil and recovery (EOR) site, where engineers used this particular characteristic of noble gases to explain the physical process of a solubility-controlled mechanism in a multi-phase system composed of gas, water, and oil phases (Bosch and Mazor, 1988; Ballentine et al., 2002; Prinzhofer, 2013). In this complex system, the noble gases were phase-partitioned at the materials' interfaces, and the noble gas compositions were mass-dependently fractionated according to their solubilities (Ballentine et al., 1991, 1994; Lollar et al., 1997; Pinti and Marty, 1995). These valuable techniques have now been extended to the study of CCS projects to monitor the migration of a multiphase CO_2 plume in the subsurface system.

Although noble gases have been actively applied in CCS research for various purposes (Myers et al., 2013), they have been largely used to identify CO_2 migration from a deep reservoir into a shallow aquifer to define a preferential pathway of migrated CO_2 and to resolve the physical interactions governing the fate of the CO_2-rich plume.

Noble gases have been used to trace CO_2 leakage in natural analogue sites and artificial injection experiments. Lafortune et al. (2009) suggested the potential applicability of noble gas for tracing gas leakage from a reservoir into a shallow groundwater system, as the reservoir has a signature of this tracer that is distinguished from that of shallow-depth groundwater. This was clearly proven at a natural analogue site of post-emplacement seepage. For example, Gilfillan et al. (2011) concluded that an elevation of HCO_3^- in shallow-subsurface and surface waters originated from deep reservoir leakage, based on a fingerprint of high-crustal ^4He. Györe et al. (2018) also pointed out that high ^4He in a deep reservoir can be used as a potential fingerprint to trace the fugitive release of reservoir gas. The concept of a noble gas fingerprint was extended to tracer-enhancement work for artificially injected CO_2 at the Cooperative Research Centre for Greenhouse Gas Technologies (CO2CRC) Otway Project to produce a strong signal for CO_2 plume leakage by distinguishing artificial CO_2 from natural CO_2 (Stalker et al., 2015).

In order to better understand the pathway of migrating CO_2 within a deep reservoir, several artificial injection experiments have been undertaken. For example, CO_2 gas was injected into a heterogeneous hydrocarbon reservoir (~3,080 m deep) within the Tuscaloosa Formation reservoir, Mississippi, United States, and was followed by continuous monitoring (Lu et al., 2012). This resulted in a unique bumpy breakthrough of noble gas having multi-peaks suggesting the existence of preferential paths between a leakage point and monitoring wells (Lu et al., 2012). In a shallow depth vadose zone injection test, preferential paths were found between the injection point and monitoring probes, as induced by the natural heterogeneity of the limestone at the DEMO-CO_2 project, France (Rillard et al., 2015). Lighter noble gases (He and Ne) were more helpful in defining the preferential path in the vadose zone than CO_2 and other tracers as they have faster arrival times at the monitoring probes owing to their higher diffusion coefficients and lower solubility within the soil water in the CO_2-Vadose project, France (Cohen et al., 2013).

Detailed and extensive research on the fate of CO_2 has been undertaken in natural CO_2-rich reservoirs, which serve as analogues for artificial CO_2 storage. For example, Zhou et al. (2005) constrained the evolution of natural CH_4 and CO_2 based on the mass-dependent fractionation of noble gases in a coalbed methane system. Studies on a natural analogue site of a deep CO_2 storage reservoir suggested that a multi-step solubility-controlled process was significantly involved in the fate of CO_2 gas under the impermeable cap-rock, as explained by the deeply fractionated noble gas ratio (Gilfillan et al., 2008; Zhou et al., 2012). Then, Gilfillan et al. (2009) concluded that naturally injected CO_2 has been primarily sequestrated within deep reservoirs through a solubility-controlled mechanism. In an engineered CO_2 injection site, Györe et al. (2015) and Györe et al. (2017) observed that the noble gas composition of produced gas can be successfully used to constrain the fate of the sequestrated CO_2 at the Cranfield enhanced oil recovery (EOR) field and identified a clear sink of free-phase CO_2 in areas making contact with the reservoir groundwater. A numerical model has also been applied to define the fate of a reservoir

of CO_2 by identifying the budget of residual trapped and immobilized gas in a deep storage site at the CO2CRC Otway test injection site (LaForce et al., 2014). Moreover, Zhang et al. (2011) delineated that immobilized gaseous CO_2 retards the arrival of noble gas tracers, owing to their preferential partitioning into CO_2 bubbles at interfaces. In a recent artificial injection experiment, an attempt was made to understand the fate of artificial CO_2 released into a shallow groundwater system (Ju et al., 2019), where the fate of the leaked CO_2 was constrained using noble gases. This highlighted the importance of solubility control and mixing mechanisms in shallow-depth groundwater.

Recently, studies have begun applying a noble gas fingerprinting tool for an actual monitoring purpose, i.e., to trace leaked CO_2 from a reservoir into a shallow aquifer system. The noble gas tracing in the shallow system is based on the inherent compositional difference between the reservoir fluid and the groundwater above, and the composition of injected CO_2 is dependent on various CO_2 capture mechanisms (Flude et al., 2016). Gilfillan et al. (2017) recognized the usefulness of composition at a real CO_2 injection site. For example, the storage reservoir was two orders of magnitude richer in radiogenic ^4He compared to normal soil gases, providing an opportunity to evaluate allegations that unplanned migration of CO_2 into a shallow aquifer near the Weyburn Midale oil fields had taken place.

Although noble gases have proved useful for tracing a CO_2 plume in many sites as described above, to the best of our knowledge, it has not yet been extensively used for monitoring in a shallow aquifer (Lee et al., 2016). Moreover, most works have been limited to artificial release experiments and natural analogue sites, implying that further efforts are still required to link the valuable previous observations to an actual CCS site. Therefore, this study attempted to discuss the application of these tracers to the monitoring of actual unplanned CO_2 migration from a CCS site. For this purpose, two injection tests were completed in a shallow aquifer system using noble gas tracers. This was intended to explain the major processes responsible for the fate of the migrated CO_2 plume in a multi-phase state and to verify the findings from previous research. Then, based on the observations, we simulated the CO_2

leakage by using analytical solutions and discussed how to use noble gas to identify CO_2 migration, and to constrain the fate of the migrated CO_2.

2 Material and methods

2.1 Artificial injection test

Sequestrated CO_2 can be mobile when the cap-rock is broken or damaged (Figure 1). Then, portions of free-phase CO_2 move upward due to buoyancy forces. Accidental leakage can occur through various vertical conduits such as an injection well, abandoned wells, or natural faults over different periods of time (e.g., continuous low level leakage or short duration blowouts) (Alcalde and Flude, 2018). While the free-phase CO_2 migrates through conduits, it can spread into the multiple layers splitting the mass (Jung et al., 2014) (Figure 1). Among the multiple layers, the ones with lower-permeabilities act as a barrier preventing the CO_2 from reaching a shallower aquifer. Following a series of stratigraphic trappings, some volumes of CO_2 finally reach the lower pressure system of shallow groundwater, which is the very portion discussed throughout this paper.

The two artificial injections were performed to demonstrate the accidental leakage of CO_2 into the shallow aquifer. In particular, the injection experiments focused on the early-stage fate of free-phase CO_2 reaching the low-pressure system (i.e. shallow aquifer). The initial state of CO_2 is characterized by a high partial pressure that can naturally nucleate the bubbles (Figure 1). The degassing dominantly occurs around a leakage point until stabilization occurs in the low-pressure system. After the degassing, the CO_2 bubbles are redistributed between the groundwater (dissolved and remaining budget) and the atmosphere (degassed and lost budget), reducing the total migrated CO_2 budget. The initial degassing is very important because it controls the overall budget of CO_2 remaining in the subsurface after it migrates into a shallower system (Ju et al., 2019). In this context, the two experiments, in which gas-charged

156 groundwater was injected into a shallow aquifer, were performed to demonstrate the early-stage
157 solubility-controlled process (i.e. degassing).

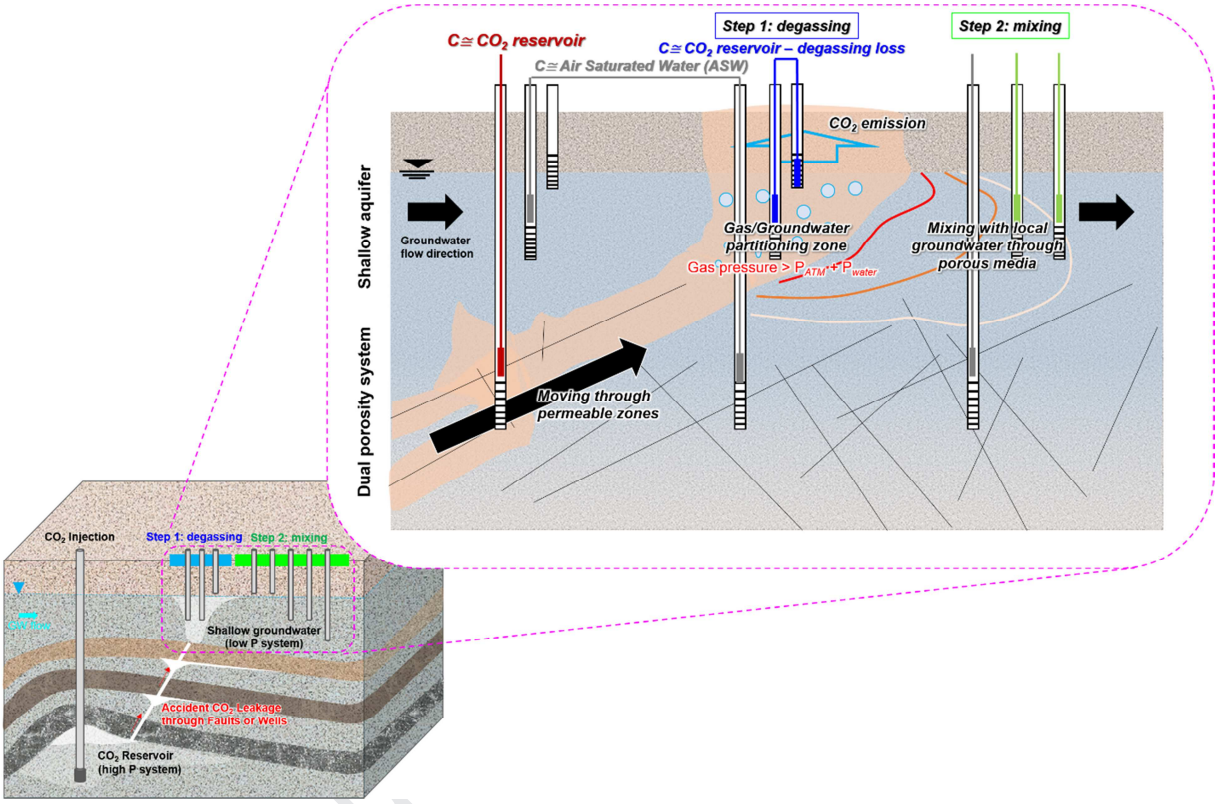

158

159 **Figure 1.** Conceptual figure to demonstrate accidental CO_2 leakage from a deep reservoir into a shallow
160 groundwater system. Early-stage fate of CO_2 is primarily controlled by the solubility-controlled process
161 (i.e., degassing) due to a high gas pressure.

162 ## 2.2 Test site overview

163 The first injection test was conducted in Wonju, Korea (Figure 1). The aquifer at the study site
164 consists of weathered and highly fractured Jurassic biotite granite overlain by soil and alluvial deposits
165 (Yu et al., 2006; Baek and Lee, 2011). The single-well tracer test (SWTT) was performed in the alluvial
166 deposits, which are a uniform material without fractures and conduits. The aquifer thickness was 10–15 m.

167 The aquifer hydrology at the site had a wide range of seasonal and spatial variations. The observed water
168 table was 2–13 m below the ground surface, but remained below 11 m during the dry season, when the
169 pilot test was performed. The hydraulic gradient varied from 0.008 m to 0.023 m. A pumping and slug
170 test revealed that the hydraulic conductivity of the site ranged between 2.0×10^{-4} cm/s and 4.2×10^{-3}
171 cm/s. In addition, the flow velocity of the regional groundwater was estimated, using ^{3}H–^{3}He analysis, to
172 vary from 1.9×10^{-6} to 1.2×10^{-4} m/s (Kaown et al., 2014). A detailed description of the geologic
173 features, seasonal variations in aquifer hydrology, and land-use history of the study site can be found in
174 Lee et al. (2015).

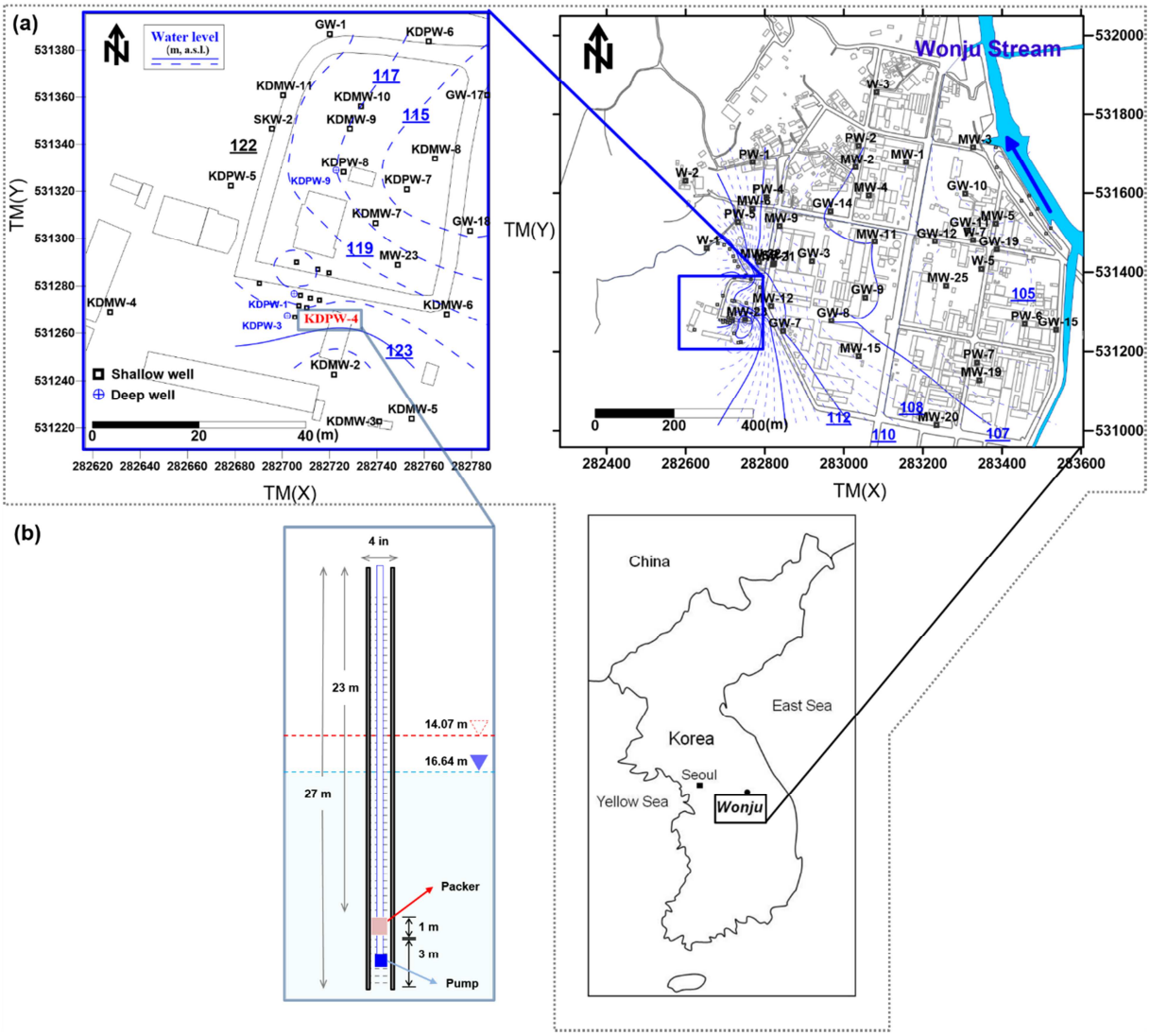

175

176 **Figure 2.** (a) Site map of Wonju, Korea; (b) full-screened KDPW4 was used for the SWTT at the site.
177 Injection was completed 24–27 m below the ground surface and approximately 10 m below the water
178 table. The injection interval was isolated using packer during the SWTT. The water table inside the
179 interval changed from 14.07 m (i.e. red triangle) to 16.64 m (i.e. blue triangle) below the surface during
180 the pull-phase of SWTT.

181 The second injection and recovery test was completed at the Korea CO_2 Storage Environmental
182 Management (K-COSEM) experimental test site in Eumseong, Korea (Figure 3). A monitoring network

was established at the test site for the CO_2 release and monitoring experiments. Geological information was collected from borehole data at the study site: an alluvial deposit was found occurring 0–2 m below ground level (b.g.l.), weathered soils were found 2–30 m b.g.l., weathered rocks were found 30–70 m b.g.l., and bedrock was found > 70 m b.g.l. (Ju et al., 2018a). The host rock was dark gray or light gray biotite granite. The inter-well tracer test (IWTT) was performed in the weathered soils zone regarded as a uniform material without any fractures and conduits. The water table was 16–17 m b.g.l., and the hydraulic gradient ranged from 0.01 to 0.05. The regional flow direction was from northwest to southeast. The hydraulic conductivity estimated from the pumping test ranged from 4.0×10^{-6} m/s to 2.0×10^{-5} m/s. A push-and-pull test was performed to identify the groundwater linear velocity (0.06–0.44 m/d), effective porosity (0.02–0.23), and uppermost aquifer thickness (47 m) of the study site. Detailed discussions on the sequential hydraulic tests for establishing the monitoring network at the K-COSEM experimental test site are summarized in Lee et al. (2017) and Lee et al. (2018).

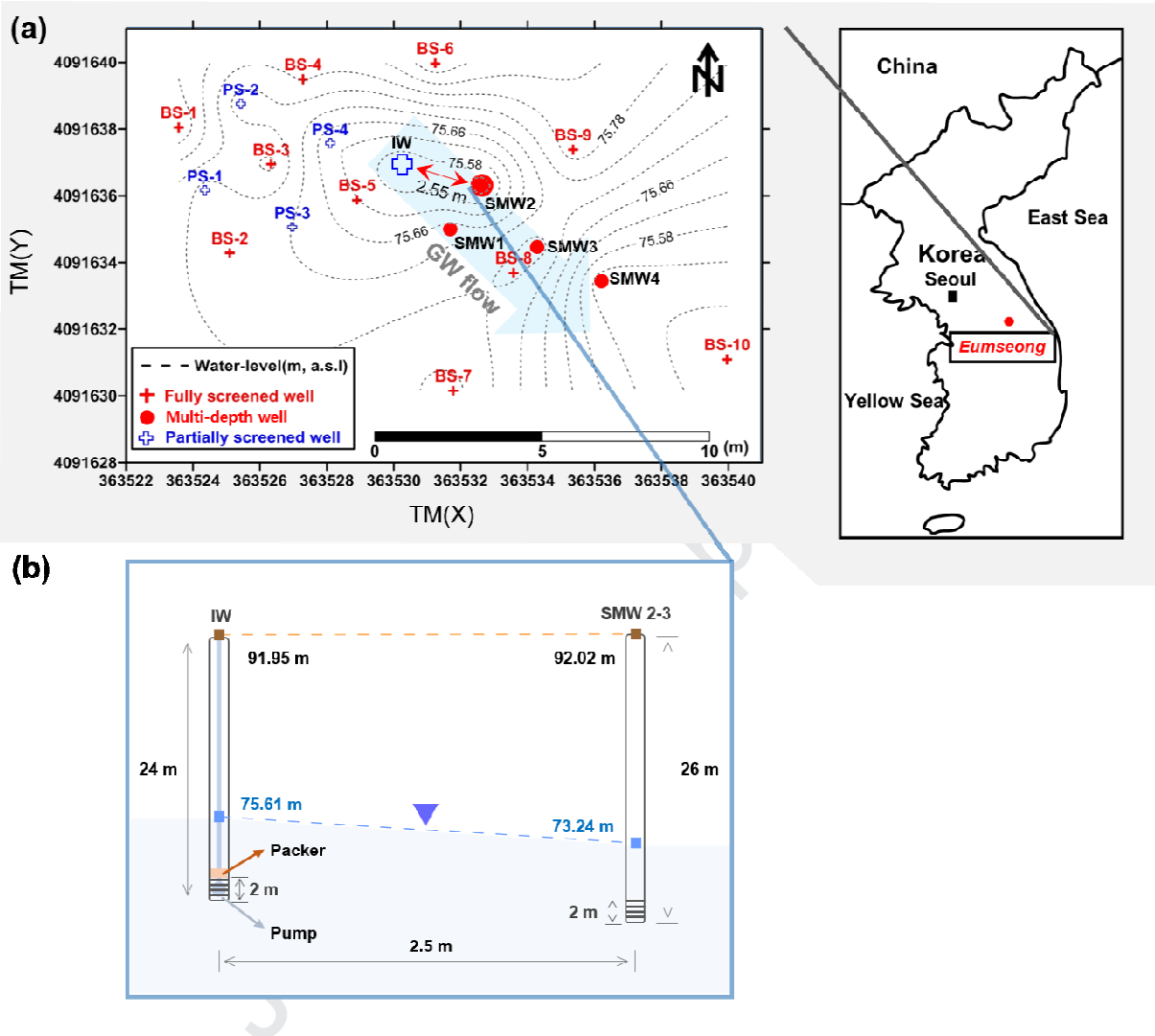

Figure 3. (a) Site map of Eumseong, Korea. (b) Injection well (IW) and saturated zone monitoring well (SMW) 2-3 were used for the IWTT. The injection was completed 21–24 m below the ground surface and 4.5–7.5 m below the water table. Injection fluid moved along an induced pressure gradient of 0.93 between the two wells.

2.3 Experimental design overview

Tracer-mixed groundwater was prepared and artificially injected into the groundwater. First, each sample of tracer-infused groundwater was created by flowing inert gases into local groundwater using a

gas regulator, ball-flowmeter, flexible tube, silencer (for gas diffusion), and carboy bottle (Figure 4). The volumes of gas-charged groundwater samples were gently mixed together in the order of their solubility in groundwater (i.e., Kr → Ar → He). The injection was completed using a submersible and controllable quantitative pump "MP1" (Grundfos, Bjerringbro, Denmark). The sample for the injection fluid (C_0) was collected during the injection period, and the salinity was measured at the sampling time using portable equipment from Yellow Springs Instruments (YSI) (YSI Inc./Xylem Inc., USA). The salinity was reported in units of ppt, with a precision of ±0.01 ppt.

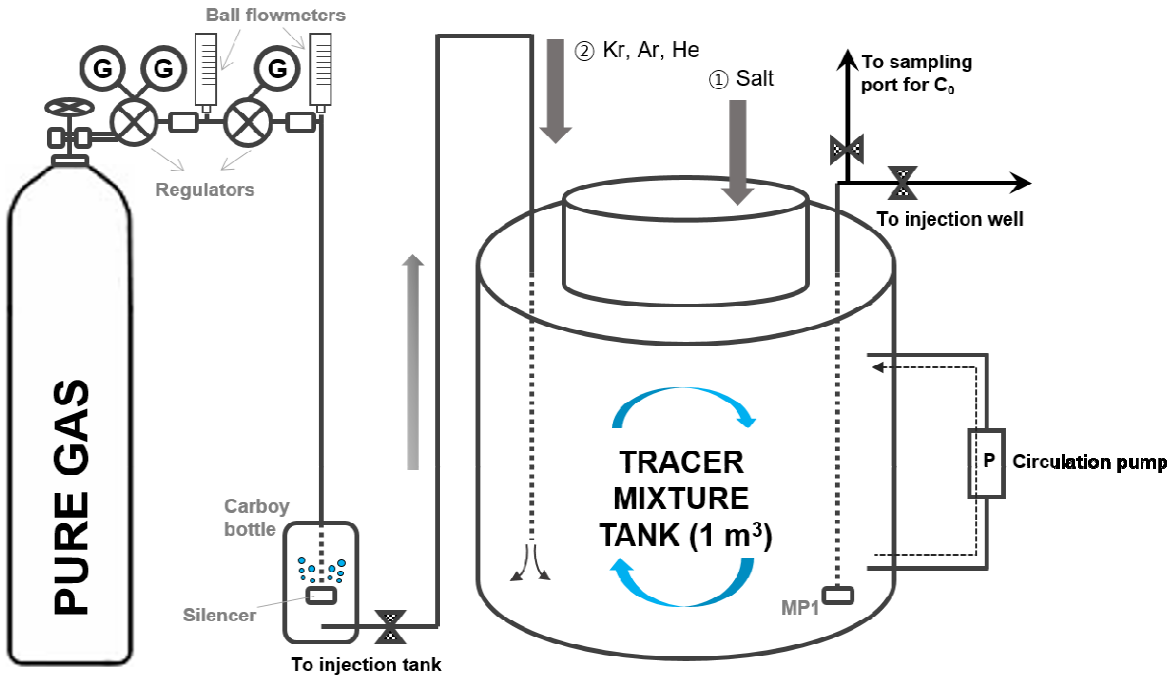

Figure 4. Schematic figure of the injection system. Volumes of tracer-infused groundwater were first prepared by blowing a pure gas (He, Ar, Kr of 99%) into the local groundwater; then, the gas-charged water samples were gently mixed together in a closed tank with a circulation pump until they were injected into the groundwater system. The injection fluid (C_0) was sampled at the sampling port attached to this tank during the injection period.

The first pilot test was carried out in Wonju, Korea, as a single-well tracer test (SWTT). The SWTT is a three-step process consisting of push, drift, and pull periods. During the push period, gas-charged groundwater (200 L) composed of salt, Ar, He, and SF_6 was injected, and was followed by the release of a chaser fluid (120 L) to flush the residual volume of injection water from the injection wellbore. The injection speed was 9.30 L/min (September 22, 2016) using KDPW4 as the injection well. This is a fully screened well with a depth of 27 m (Figure 1). The target injection zone was 24–27 m below ground level, and 10 m below the water table. A packer was used to tightly seal the area 1 m above the target injection zone. After the injection period, the tracer-infused water had a drift time of 1,522 min in the groundwater system. Then, in the pull period, it was recollected for 319 min at a rate of 3.87 L/min through the injection well (September 23, 2016). At the same time, parts of the pulled groundwater were sampled at the well surface. The samples of the inert gas tracers were collected at 2–10 min intervals that were gradually increased. The salinity was measured *in situ* using portable equipment from YSI (YSI Inc./Xylem Inc, USA) every 2–10 min, and this interval was also gradually increased.

The second pilot test was performed at the K-COSEM experimental test site as an inter-well tracer test (IWTT). Before the tracer injection, an induced hydraulic gradient of 0.93 was created between the injection well (IW) and saturated zone monitoring well (SMW) 2–3 (Figure 3). Gas-charged groundwater (1,000 L) composed of salt, Kr, Ar, and He was released into the IW at a rate of 4.74 L/min (October 13, 2016). The target injection zone was 21–24 m below the ground surface, and 4.5–7.5 m below the water table at IW. The injection event was followed by 10 days of monitoring at the SMW 2-3 of down gradient (to October 22, 2016). Parts of the pulled groundwater were sampled at the well surface of SMW 2-3. The samples for the inert gas tracers were collected in 2–5 h intervals that were gradually increased. The salinity was measured *in situ* using portable equipment from YSI (YSI Inc./Xylem Inc, USA) every 2–5 h, and this interval was also gradually increased.

2.4 Data acquisition from water samples

The groundwater samples for sulfur hexafluoride (SF_6) were collected in glass bottles and were tightly sealed using caps with metal liners. The sample analysis was automatically completed at the Core Laboratory of Innovative Marine and Atmospheric Technology (CLIMATE) at the Pohang University of Science and Technology (POSTECH). The automatic device included a gas chromatograph equipped with an electron capture detector, a SF_6-extraction device, a global positioning system, and a data acquisition system based on Visual Basic 6.0/C 6.0. The SF_6 in the groundwater was quantified in comparison to gas standards of 6, 60, 103, 104, 200, 352, and 704 pptv. The precision of this method was better than 0.2% (Koo et al., 2005).

For noble gas analysis, 28 cm^3 of groundwater was sampled using a copper tube and a stainless-steel clamp (to prevent air contamination). The samples were analyzed in the noble gas analysis laboratory at the Korea Polar Research Institute (KOPRI). First, the dissolved gas was extracted from the groundwater under a high vacuum (~10^{-7} mbar) and stored in an aluminosilicate ampoule to remove the majority of the water in a manner similar to the method of Lott and Jenkins (1998). The extracted gas was further treated using a separated and automated processing line equipped with cryogenic traps and getter pumps (hot and cold St 101, SAES) (Beyerle et al., 2000) as outlined in Stanley et al. (2009) to remove residual water vapor, active gases, and other condensable gases. Then, each noble gas component was cryogenically separated and drawn down into a mass spectrometer, i.e., a residual gas analyzer (RGA) 200 (Stanford Research Systems, California, USA), from low mass to high mass. ^{4}He, ^{40}Ar, and ^{84}Kr were quantified and calibrated against air standards of 0.9–2.7 cm^3 in consideration of the wide concentration range of artificially enhanced tracers. Then, the abundant isotopes were reported as the total amount of each noble gas at standard temperature and pressure (STP), assuming they are isotopically air-like. The analytical error for the post-injection data was less than 5% based on duplicate sample analyses (Ju et al., 2018b, 2019).

3 Results

3.1 Tracing artificially leaked plume

The noble gas tracer method has shown the potential to explain the fate of high-pressure CO_2 that has migrated from a deep reservoir into a shallow aquifer system (Gilfillan et al., 2017; Ju et al., 2019). In this section, the behavior of the noble gas was determined following the two separate controlled release experiments in the shallow-depth aquifer system. Specifically, during the two injection tests, the mass recovery was observed after injecting the groundwater charged with the partitioning (i.e. inert gas tracers) and non-partitioning tracers (i.e. salt) into the shallow aquifers. Here, the partitioning tracer is defined as a substance having a partitioning behavior in a multi-phase system composed of gas and groundwater and, the non-partitioning tracer only exists as a dissolved phase in the multi-phase system.

3.1.1 Mass recovery curve of the leaked plume

A total of 200 L of groundwater (C_0) containing 68.6 ppb of SF_6, 2.05×10^{-6} cm^3 STP/g of He, 3.06×10^{-3} cm^3 STP/g of Ar, and 10.7 ppt of salt was injected into the shallow aquifer. The mass recovery of the inert gas tracers was calculated in an identical manner as Kim et al. (2018), where the total recovery was a summation of the areas in a volume-concentration plot (i.e., recovery = Σ volume (L^3) × concentration (M/L^3)). The results revealed that the recovery ratio of each tracer was clearly related to its respective solubility. As shown in Figure 5a, the recovery ratios of SF_6, He, Ar, and salt were 49.3%, 58.1%, 78.2%, and 73.1%, respectively. The solubility-controlled processes of phase-partitioning and degassing influenced the fate of the injected gas tracers as expected (Ballentine et al., 2002). The tracer recovery ratios from single-well push-pull tracer tests exhibited various ranges of distribution depending on the nature of tracers, drift time, pump back rate, and density effect, and several controlled tests revealed that the recovery ratios do not reach 100% (Kim et al., 2018). Although salt is known to be conservative in a groundwater system, the mass recovery of salt was slightly less than that of the Ar tracer.

286 As salt does not undergo phase-partitioning in a groundwater system, entrapment of salt mass into low
287 permeability zones was a possible reason for the mass loss in the SWTT (Kim et al., 2018, 2019).

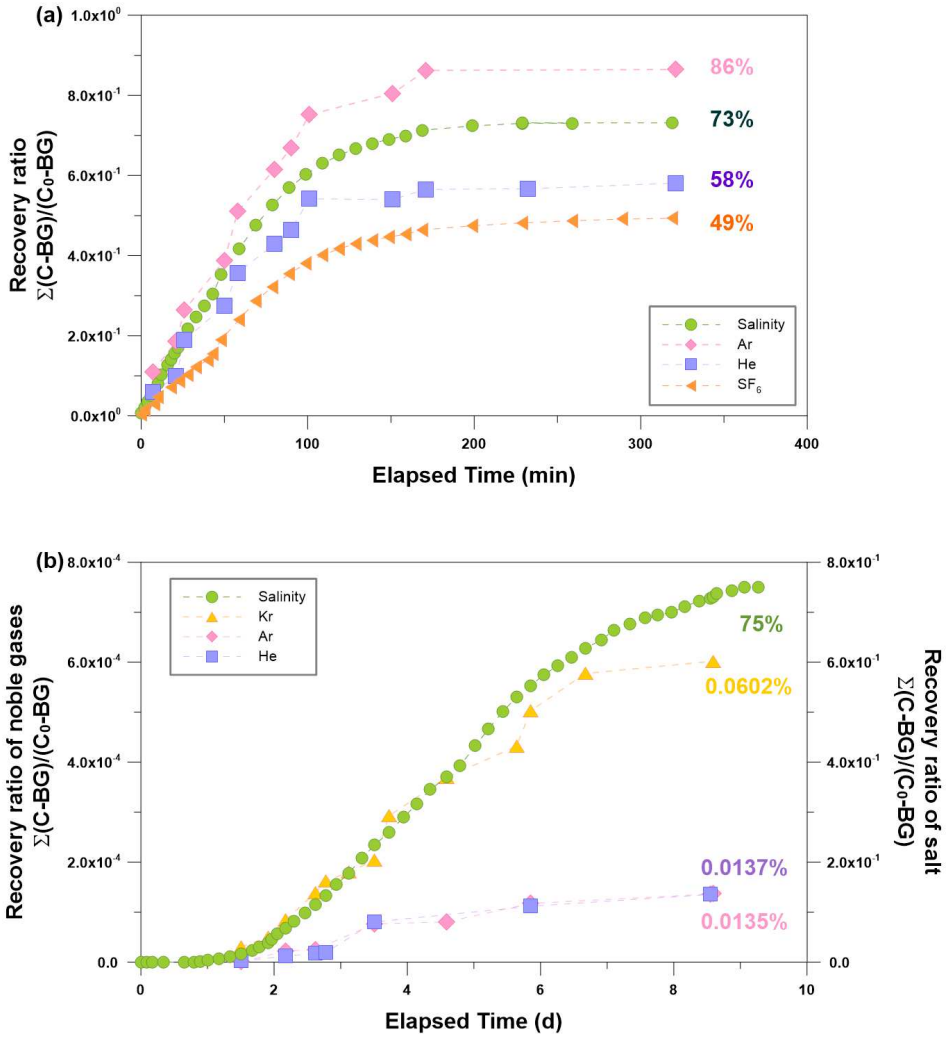

288

289 **Figure 5.** Mass recovery curves of the injected tracers (a) from the SWTT and (b) from the IWTT. Each
290 Y-axis displays the recovery ratio of tracers recorded above the background level. The recovery rate of
291 inert gas tracers was relative to their solubility for groundwater in an air-water system, indicating that
292 solubility-controlled processes were involved in the fate of the leaked plume.

A total of 1,000 L of groundwater containing 4.02×10^{-6} cm^3 STP/g of He, 2.29×10^{-2} cm^3 STP/g of Ar, 1.05×10^{-5} cm^3 STP/g of Kr, and 5.87 ppt of salt was injected into the shallow aquifer. The mass recovery rate of the IWTT was much lower than that of the SWTT. In particular, the difference between the non-partitioning tracer (i.e., salt) and the partitioning tracers (i.e., noble gas tracers) in terms of mass recovery was much greater than that of the SWTT, in which the mass recoveries of He, Ar, Kr, and salt were 0.0135%, 0.0137%, 0.0602%, and 75.0%, respectively. The non-partitioning tracer flows along the groundwater flow paths, and only a portion of the tracer mass is not captured in the recovery well because of dispersion or density-effect (Kim et al., 2018). In contrast, the partitioning tracers can easily escape from the flow paths, owing to their high diffusivity and partitioning behavior (Carrigan et al., 1996; Heilweil et al., 2004), resulting in a significant decrease in the mass recovery (see next section). Specifically, the extremely low level of recovery for the noble gas tracers, which was three orders of magnitude lower than that of salt, seems to be attributable to several factors related to the design of the experiment: 1) the brine had been charged with insoluble tracers for several hours; therefore, it is possible that the total gas pressure of injected water increased beyond $P_{ATM} + P_{H2O}$ at the injection point, resulting in active bubble growth; 2) the pumping action at the extraction well (i.e., SMW 2-3) possibly induced a pressure drop, accelerating the bubble growth; 3) the upward movement of the injected plume toward the water table through the permeable materials of the borehole resulted in a re-equilibrium of the high P plume (i.e. gas-charged water) with the atmosphere. Istok et al. (2006) highlighted the degassing mechanism of a high P plume through borehole materials in detail. The mass recovery ratios of the partitioning tracers, however, were clearly in the order of their solubilities for groundwater (Table A.1 in Appendix A). Therefore, solubility-controlled processes influenced the fate of the gas-charged plumes during the IWTT (Ballentine et al., 2002).

3.1.2 Fate of the leaked plume

316 In the mass recovery curves, the recovery ratios of the noble gas tracers followed the order of the
317 tracers' solubilities in groundwater, suggesting that solubility-controlled processes influenced the
318 migration of the leaked plume. The Rayleigh distillation equation was used to explain the influence of the
319 solubility-controlled processes on the fate of the leaked plume (Ballentine et al., 2002). The equations for
320 estimating the degassing process are listed in Appendix A, where the partitioning coefficients in pure
321 water system were adopted for the calculation (Table A.1). A continuous degassing of the He and Ar
322 tracers is apparent, as shown in Figure 6 (i.e., the gray arrow). Without the degassing loss, the tracers
323 were expected to follow the mixing line between the injection and background concentration (i.e., the
324 dashed line for Figure 6a and dash-dot line for Figure 6b). However, once the degassing process starts, the
325 noble gas composition of the dissolved plume fractionates, because less soluble and lighter elements are
326 preferentially lost into the gas phase at the gas/water interfaces than those that are heavier (Ballentine et
327 al., 2002). As shown in Figure 6, the He/Ar changed relative to the tracer's solubility, following the
328 degassing line (i.e., gray arrow). During the SWTT, the noble gas distribution was defined by the two
329 physical processes such as the degassing and mixing processes. The two processes could not be explained
330 separately, as the concentration change arose from both mechanisms occurring at the same time (Figure
331 6a). This seemed to be attributable to the experimental procedure of the SWTT, in which the three-step
332 process (push-drift-pull) caused multiple stress periods (e.g. pressure instability/vertical movement) that
333 caused the dissolved plume to irregularly degas as the local groundwater diluted the multi-phase plume.

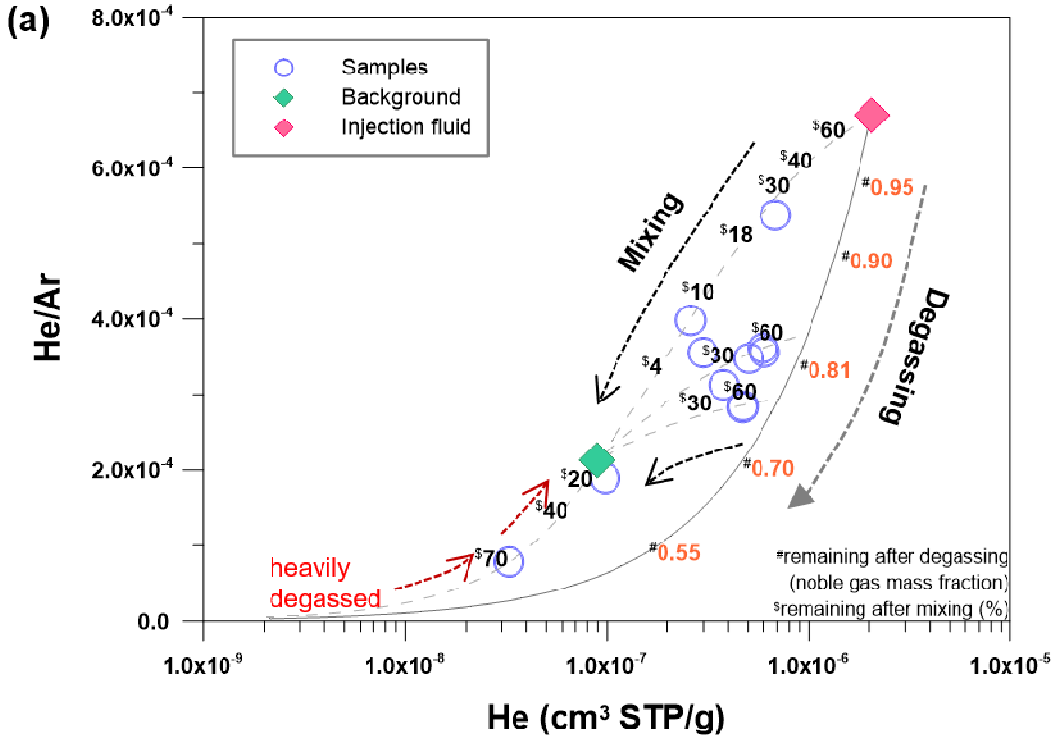
(a)
Samples
Background
Injection fluid
Mixing
Degassing
heavily degassed
#remaining after degassing (noble gas mass fraction)
$remaining after mixing (%)
He/Ar
He (cm³ STP/g)

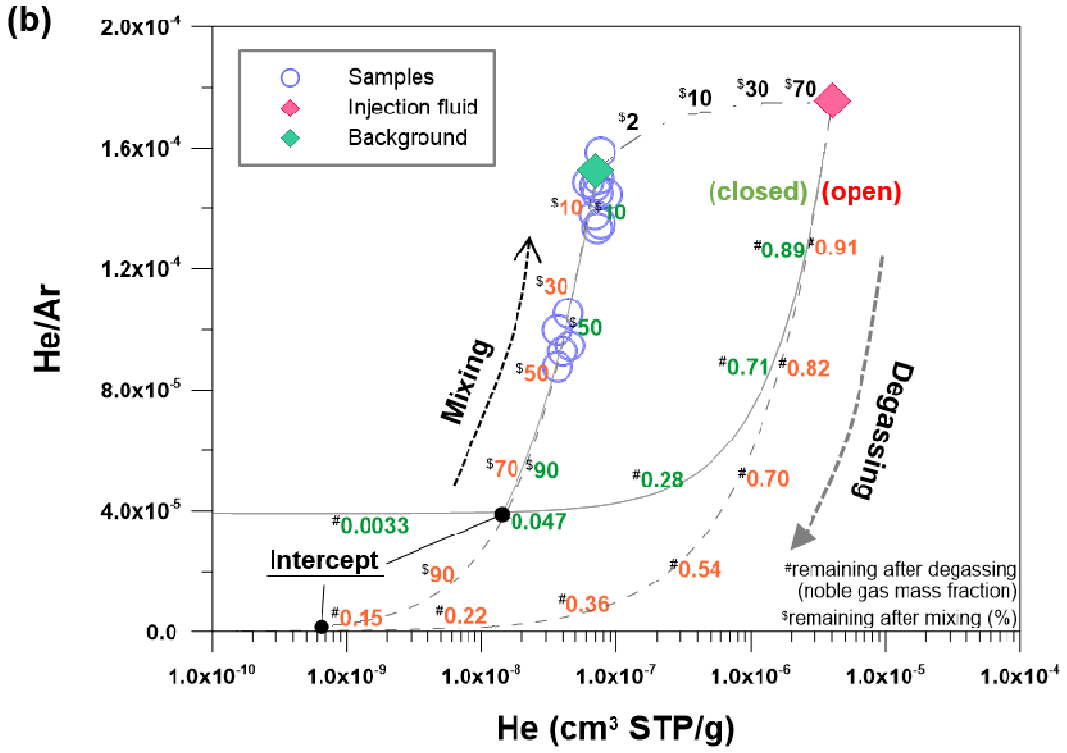
(b)
Samples
Injection fluid
Background
(closed)
(open)
Mixing
Degassing
Intercept
#remaining after degassing (noble gas mass fraction)
$remaining after mixing (%)
He/Ar
He (cm³ STP/g)

334

335 **Figure 6.** (a) Noble gas concentration anomaly of the SWTT. The injected tracer changed with both the
336 degassing and mixing processes. The two processes occurred concurrently and could not be explained
337 separately. The heavily degassed sample spent the longest time in the groundwater system, showing the
338 bottom upward recovery toward background levels. (b) Noble gas concentration anomaly of the IWTT.
339 The degassing process first occurred and was followed by a mixing process. The mass retention and loss
340 of the tracer gases can be evaluated in either an open system (orange colored) or a closed system (green
341 colored) at the intercept (see the text for details).

342 Two distinctive models were employed to explain the mass retention and the loss of injected
343 tracers during the IWTT (Ballentine et al., 2002; Gilfillan et al., 2008; Ma et al., 2009). The first is the
344 degassing of tracers in a closed system, in which air bubbles are retained and trapped in a groundwater
345 system following the degassing process. In a closed system, equilibrium is achieved between the gas
346 phase and the dissolved phase in the groundwater at the end of the degassing process. The second is
347 phase-partitioning in an open system, in which the degassing process results in a mass reduction in the
348 total mass. Consequently, air bubbles, having mobility, are lost into the atmosphere following the phase-
349 partitioning. In an open system, the air mass is lost into the atmosphere stepwise until the end of the
350 degassing process. Both of these extreme cases were modeled and elucidated for the fate of injected fluid
351 during the IWTT (Appendix A). In Figure 6b, phase-partitioning in the closed system is denoted by a gray
352 line and that in the open system is depicted by a gray dotted line.

353 The two processes (i.e., degassing and mixing) were separated in the time domain during the
354 IWTT, in which the degassing process occurred first and was followed by the mixing process, unlike in
355 the SWTT. The separation of the two processes gave us an opportunity to quantify the degassed amount
356 (Zhou et al., 2005). At the intercept, the gas/water ratio was 2.44 for the closed system and 0.162 for the
357 open system. As the shallow groundwater cannot hold such a large amount of gas (gas/water = 2.44) in
358 the system, the environment behaved like an open system during the degassing process. Then, the gas

359 volume liberated from water was constrained at the intercept of the open system and reached 0.162×10^6
360 cm^3 (Figure 6b) (Appendix A). This amount corresponds to the residual Ar of 3.61×10^{-4} cm^3 STP/g in
361 groundwater that is already close to the ASW level (3.60×10^{-4} cm^3 STP/g) in an aquifer system,
362 suggesting the injected plume depressurized and stabilized in the local system even before interacting
363 with local groundwater.

364 **4 Discussion**

365 Noble gas tracers were employed for two injection tests to explain the physical processes
366 involved in the migration of a leaked plume, i.e., gas-charged water, in a shallow aquifer system. During
367 the tests, the fate of the leaked plume was first defined by a solubility-controlled process (i.e., degassing),
368 which was followed by a volumetric mixing process. This result is consistent with observations from
369 another artificial injection test (Ju et al., 2019), which revealed that the noble gas anomaly in a CO_2-rich
370 plume is a function of the degassing and physical mixing processes in a shallow aquifer system (see
371 Figure 11 in Ju et al., 2019). Furthermore, these are similar to the conclusions reached at a natural CO_2
372 production site (Zhou et al., 2005) that stripping loss of insoluble gases was followed by dilution by
373 diffusive mixing with the un-degassed local groundwater. These observations suggest that the solubility-
374 controlled process and the mixing process are primarily responsible for the fate of the leaked plume in the
375 shallow aquifer system.

376 **4.1 Application of a noble gas tracer to the detection of CO_2 leakage: Case study at the**
377 **Weyburn and Midale oil fields**

378 Noble gas tracers have been applied to study the fate of leaked CO_2 in a shallow aquifer system
379 (Gilfillan et al., 2011; Ju et al., 2019; Zhou et al., 2005). However, previous studies have been sparingly
380 applied to artificial injection tests and natural analogue sites. Although these works provide an insight on
381 the behavior of a leaked plume, further efforts are required to link those valuable observations to an actual

CCS site. Specifically, we need to know what we would observe if the free-phase CO_2 accidently reached the shallow aquifer. This can be demonstrated by simulating the hypothetical leakage on an actual CCS site based on our observations from the two distinct artificial injection tests and other valuable previous studies. To understand the fate of CO_2 under hypothetical leakage conditions, the monitoring data from the Weyburn storage site was incorporated in the leakage simulation.

The Weyburn Midale oil field is a CO_2-EOR and CO_2 storage site, where a large amount of CO_2 has been introduced into a deep reservoir (Gilfillan et al., 2017). Recently, this site received public attention as CO_2 leakage allegations implying that anthropogenic CO_2 leaked from the deep reservoir into a nearby shallow aquifer on private land were made. At this site, Gilfillan et al. (2017) used the inherent noble gas tracers in the different fluids associated with the site to judge whether upward migration had occurred from the deep reservoir into the shallow aquifer. Based on the results, the leakage allegation (i.e., upward migration of CO_2) were proved false, as the observed concentration of noble gas tracers simply did not follow the composition of the reservoir CO_2 carrying the high amount of radiogenic ^4He (see Table 1 for the composition of two reservoirs).

Though this case study proved the usefulness of a noble gas tracer, we have expanded this study in a more quantitative way to discuss what we would actually observe if free-phase CO_2 leaked into a shallow aquifer. Repeated simulations were made based on various analytical models to understand how we can use a noble gas tracer as a proxy to understand the fate of free-phase CO_2 that has leaked from a deep reservoir into a shallow aquifer system.

401 **Table 1** Noble gas composition in shallow groundwater and in a CO_2 plume. The noble gas distribution of
402 dissolved CO_2 was calculated based on the composition of gas produced from the Weyburn storage
403 reservoir. Note that the composition of the shallow aquifer is close to that of the air saturated water
404 (ASW).

	^{4}He ($\times10^{-8}$)	Ne ($\times10^{-7}$)	^{20}Ne ($\times10^{-7}$)	^{40}Ar ($\times10^{-4}$)	^{36}Ar ($\times10^{-6}$)	^{84}Kr ($\times10^{-8}$)
Dissolved CO_2, C_0 [†]	763	0.084	0.076	0.724	0.138	1.440
(std dev.) [‡]	1831	0.135	0.123	0.986	0.186	0.344
	58.2	32.9	33.1	21.7	21.0	86.9
Shallow Aquifer [§]	5.84	1.90	1.73	3.04	1.03	4.92
(std dev.) [‡]	29.1	18.5	18.3	9.24	8.96	11.2
ASW [¶]	4.25	1.81	1.64	3.25	1.10	4.29

405 All the measured data were from Gilfillan et al. (2017) in cm^3/g.

406 [†]noble gas contents in dissolved CO_2 prior to stripping loss calculated assuming 100% dissolution of the
407 free-phase CO_2 at the P and T conditions of shallow groundwater; temperature of 14.3°C, salinity of 0.02
408 g/kg, and pressure of 0.101 MPa. The high level of ^{4}He in the dissolved CO_2 is attributed to an interaction
409 between the reservoir gas and crustal sources. The depletion of the other noble gases is due to an
410 interaction between the reservoir gas and artificially injected CO_2.

411 [‡]1 sigma value relative to the average (%).

412 [§]average concentration of noble gases in the shallow groundwater samples.

413 [¶]Air saturated water (ASW) concentration was calculated assuming a temperature of 14.3°C, salinity of
414 0.02 g/kg, and altitude of 580 m.

415 **4.1.1 Fate of free-phase CO_2 in the shallow aquifer**

Previous studies have revealed that diverse factors control the noble gas composition of captured CO_2 once it is injected into the subsurface, such as the initial capture process, degassing, dissolution, diffusion, adsorption, CO_2 density, and reservoir interactions (e.g., with atmospheric, crustal, and mantle sources) (Flude et al., 2016; Gilfillan et al., 2011; Holland and Gilfillan, 2013; Kilgallon et al., 2018; Warr et al., 2015; Wilkinson et al., 2010; Zhou et al., 2005). Furthermore, a recent artificial release test demonstrated the behavior of leaked CO_2 in a shallow aquifer, which was defined by degassing and mixing processes based on noble gas tracers (Ju et al., 2019). From the insights of previous works, we will discuss how these processes are involved in the fate of free-phase CO_2 in a shallow aquifer system based on the behavior of noble gas tracer.

The free-phase CO_2 that leaks from a deep reservoir into a shallow aquifer is rich in ^{4}He from previous interactions with a deep crustal source but is low in other elements from the initial industrial capture process (Table 1). Following leakage, free-phase CO_2 forms a dissolved plume in a shallow aquifer, and the contents of the plume naturally follow those of the free-phase CO_2. The concentration of the CO_2 plume (i.e., the blue cross symbol) will change in the groundwater system depending on various physical interactions, which are depicted using the ^{4}He and ^{40}Ar tracers in Figure 7. A detailed description of the theoretical calculations can be found in Appendix A. One of most noticeable processes controlling the fate of this plume is a volumetric mixing process (Gilfillan et al., 2011; Ju et al., 2019) (see also Figure 6) occurring as the CO_2 plume moves through porous media with the local groundwater. While being gradually mixed with the local groundwater, the initial plume becomes depleted in ^{4}He and enriched in ^{40}Ar (i.e., the black line). The noble gas anomaly in this process is dependent on the compositional difference between the initial plume and local groundwater, and their mixing fractions, whereby ^{4}He could vary by up to -99.6% and ^{40}Ar could vary by up to 256% (i.e., the light gray zone).

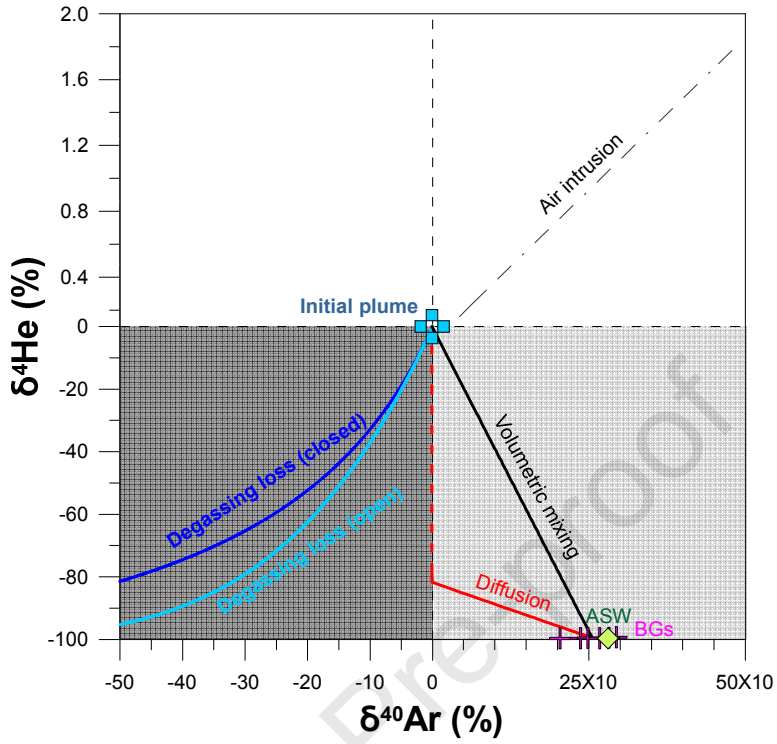

438

439 **Figure 7**. Percent change in the noble gas concentration (i.e., [NG – NG_i] / $NG_i \times 100$) from the initial
440 composition (NG_i) under various physical processes. The composition of the initial plume was calculated
441 assuming 100% dissolution of free-phase CO_2 in the shallow aquifer (see Table 1). BGs (i.e., pink cross
442 symbols) present the concentrations of shallow aquifer samples, and ASW is the air saturated water
443 concentration under local groundwater conditions (i.e., green diamond; see Table 1). In the light gray
444 zone, the mass distribution is controlled predominantly by mixing processes. Volumetric mixing occurs as
445 the CO_2 plume moves through a porous medium with the local groundwater (i.e., the black line)
446 (Appendix A). The diffusion process occurs along a concentration gradient, for example, at a plume
447 boundary or water table (i.e. the red line) and is depicted with diffusion coefficients from Jähne et al.
448 (1987) and Wise and Houghton (1966) (Eq. A.4 in Appendix A). It only occurs at $t > 4\pi D$, theoretically
449 (i.e., the dotted line before threshold) (Fetter, 1999). The dark gray zone indicates a large contribution of a
450 solubility-controlled process to the fate of the CO_2 plume. The degassing process occurs during the initial

period of a leakage and continues until the plume is stabilized in the relatively low pressure condition of the shallow aquifer (i.e., the blue and light blue lines) modeled using partitioning coefficients from the NIST chemistry webbook of Sander (2017) (Appendix A). Explanations for each degassing system (i.e., closed and open) can be found in the text. The air intrusion line depicts the data contamination due to the addition of atmospheric air into groundwater during the sampling procedure (i.e., the black dotted line). All the measured data were from Gilfillan et al. (2017).

Diffusive movement occurs along the concentration gradient under Fick's second law and would be observable at the plume boundary where the CO_2 plume meets the local groundwater. This also occurs at the water table, when the plume makes contact with the atmosphere. Therefore, in these places (i.e., plume boundary and water table), the composition of the noble gas will be differentiated from that of the plume center (i.e., the red line in Figure 7). The maximum change (%) is, however, consistent with the volumetric mixing process, as this process is also based on the concentration difference between the CO_2 plume and local groundwater. The diffusion process affects the fate of dissolved gas plume at a natural gas production site (Zhou et al., 2005). With the gas production, there was an intensive stripping loss of insoluble noble gases, which resulted in a steep concentration gradient at a contact boundary where noble gas tracers diffusively spread along a concentration gradient. In a fractured aquifer, this process can result in significant loss of insoluble noble gases into immobile zones because of a concentration gradient between the mobile (i.e. fractures) and immobile zones, and therefore, a delay of lighter elements observable at monitoring points (Carrigan et al., 1996; Sanford et al., 1996). Moreover, this behavior was minutely demonstrated in a numerical simulation following a detailed laboratory experiment (Kilgallon et al., 2018), in which the arrival time of the noble gas was determined predominantly by the diffusion process while migrating in a gas phase CO_2.

In contrast, a solubility-controlled process leads to a depletion of all tracers (i.e., the dark gray zone in Figure 7). This process is possibly observable at the initial stage of leakage when the CO_2 plume

475 is unstable owing to the high partial pressure of inherent gases (Figure 1). The initial plume would degas
476 the CO_2 rapidly until it stabilized in the lower pressure of the shallow groundwater, as shown in the IWTT
477 (Figure 6b). During this process, the free CO_2 carries the insoluble gases from the dissolved phase and
478 stays in the surrounding environment, resulting in a gas–water equilibrium (closed) or CO_2 bubbles of
479 infinitesimally small size escaping from the groundwater continuously until the end of degassing process
480 (open) (Ballentine et al., 2002; Gilfillan et al., 2008; Ma et al., 2009). This process results in the noble
481 gases fractionate continuously until the plume is stabilized at local conditions of P, T, and CO_2-density in
482 shallow groundwater. It is evident that the lighter ^{4}He tends to be more depleted compared to the heavier
483 ^{40}Ar, and this trend appears more significant in the open system than in the closed system (dark gray
484 zone). The solubility-controlled process is a major mechanism controlling the fate of a CO_2-rich plume,
485 and has been observed in a natural analogue site of CO_2 leakage (Zhou et al., 2005) and an artificial CO_2
486 injection experiment (Ju et al., 2019), in addition to the current experiments.

487 The adsorption process is known to result in a relative enrichment of heavy noble gases (i.e. Kr
488 and Xe) in terrigenous sediments (Fanale and Cannon, 1971), and this phenomenon is particularly
489 noticeable in a system that includes organic rich units such as shale formation (Podosek et al., 1981).
490 Should groundwater or free-phase CO_2 makes contact with such an organic rich formation, it will become
491 enriched in heavier species (i.e., Kr and Xe) from the ASW composition, reflecting the release of
492 sedimentary noble gases (i.e., heavier species) from the organic source kerogens (Torgersen et al., 2004).
493 The action of this process has been demonstrated in organic rich sediments, where the distribution of the
494 heavier species can be distinguished from those of a normal oil-water system (Torgersen and Kennedly,
495 1999) and gas-water system (Ma et al., 2009). Unfortunately, proper coefficients had not been provided
496 for this mechanism (Holland and Gilfillan, 2013; Myers et al., 2013; Flude et al., 2016), and inevitably,
497 an analytical calculation was not made for this process. However, groundwater that makes contact with
498 organic matter evidently becomes enriched in heavier noble gases (i.e. Kr and Xe); therefore, samples

499 affected by this process should be carefully treated, and lighter species (i.e. He, Ne and Ar) should be
500 adopted for the other quantitative evaluations.

501 The air intrusion line depicts data contamination due to the addition of atmospheric air into
502 groundwater during the sampling process. The effects of air contamination are very different from the
503 other processes, as air contamination results in positive changes for both elements (i.e., the right-side of
504 the white zone in Figure 7). This suggests that we can possibly distinguish and separate this erroneous
505 behavior for quantitative evaluations.

506 **4.1.2 Monitoring efficiency of noble gas tracers**

507 As noble gas analysis is time-intensive, people who want to use these tracers for monitoring CO_2
508 leakage will naturally wonder which tracer is most efficient. It seems evident that the tracer showing the
509 largest compositional difference between the free-phase CO_2 and shallow system would be the most
510 efficient for tracing CO_2 leakage in a shallow aquifer (Flude et al., 2016). In that regard, the tracer with
511 the largest difference in concentration between the C_0 (i.e., dissolved CO_2 from Table 1) and BG (i.e.,
512 shallow aquifer from Table 1) can easily detect CO_2 in the monitoring system. In addition to the
513 compositional difference, the natural variation is another factor controlling the monitoring efficiency. In
514 terms of leakage monitoring, the natural variation of monitoring parameters can dilute the leakage signal
515 and deteriorate the monitoring efficiency. For this complicated issue, Risk et al. (2015) defined a
516 minimum threshold value for each monitoring parameter to confirm CO_2 leakage safely. According to
517 previous research, a "leakage" could be detected safely when signals of a monitoring parameter increase
518 over the three sigma value of the natural variation of the parameter. In Table 2, the threshold values (3σ)
519 are listed for each tracer.

520 **Table 2** Conditions for detecting the CO_2 leakage in a monitoring system. A large difference in noble gas
521 composition between the C_0 (i.e., dissolved CO_2 from Table 1) and the BG (i.e., shallow aquifer from

Table 1) indicates a high monitoring efficiency. The CO_2 leakage will be recorded in a monitoring system for the first time when the concentration starts to increase/decrease over the 3σ value, which was calculated for each element (upper section). Each cell in bottom section indicates the minimum proportion of CO_2 plume arriving at a monitoring system needed to overcome the detection threshold (i.e., the value corresponding to the 3σ value in Figure 8) calculated for various cases of degassing loss. Note that the large difference in ^{4}He content between the C_0 and BG will generate a huge signal that will be larger than the 3σ value with a small portion of CO_2 arriving at a monitoring point. Therefore, a high monitoring efficiency will be achieved.

	^{4}He	^{20}Ne	^{40}Ar	^{36}Ar	^{84}Kr	^{4}He/^{40}Ar	^{84}Kr/^{20}Ne
	($\times10^{-8}$ cm^3/g)	($\times10^{-7}$ cm^3/g)	($\times10^{-4}$ cm^3/g)	($\times10^{-6}$ cm^3/g)	($\times10^{-8}$ cm^3/g)	($\times10^{-3}$)	-
$\lvert C_0\text{-BG}\rvert^{\dagger}$	1292	1.63	2.19	0.865	4.03	152	0.601
3σ of BG‡	5.09	0.95	0.84	0.276	1.65	0.123	0.210
Degassing Amount¶	---------- mixing % with CO_2 plume§ ----------						
0	0.394	58.4	38.6	31.9	41.0	0.00288	5.64
1.8	1.14	56.4	35.6	30.7	40.0	0.00823	5.18
4.5	5.78	55.4	32.8	29.4	38.7	0.04	5.57
7.2	37.4	55.1	31.1	28.6	37.7	0.198	6.44

All the measured data were from Gilfillan et al. (2017).

†difference in noble gas concentration between the initial CO_2 plume (C_0) and the shallow groundwater (BG). Note that a large difference indicates a high monitoring efficiency.

‡3 standard deviation of shallow groundwater samples, presenting the natural variability.

¶degassed amount from a CO_2 plume in an open system in units of $\times10^{-7}$ cm^3 STP/g.

535 [§]At least n% of the CO_2 plume should arrive at the monitoring system to override the detection threshold
536 (i.e., the 3σ value) and so that CO_2 leakage can be reported. This concept was introduced by Risk et al.
537 (2015).

538 **4.1.2.1 Physical processes affecting the monitoring efficiency**

539 As noble gas distribution is related to physical interactions in the CO_2 leakage condition (see
540 section 4.1.1. Fate of free-phase CO_2 in shallow aquifer), the monitoring efficiency of noble gas tracers is
541 also dependent on physical processes. When CO_2 leakage occurs in a shallow aquifer, one can first
542 observe the front of the CO_2 plume at a monitoring well as it gradually approaches the monitoring areas.
543 In this case, the "first signal" of the noble gas parameters will be variable, depending on the nature and
544 magnitude of the physical processes controlling the evolution of the CO_2-rich plume. The evolutionary
545 path of the CO_2 plume was depicted using noble gas tracers under physical processes (Figure 8), and was
546 based on observations made from two iterations of artificial injection tests and previous studies (Gilfillan
547 et al., 2011; Ju et al., 2019; Sanford et al., 1996; Zhou et al., 2005). In this scenario, the initial CO_2 plume
548 is unstable, owing to the high partial pressure of CO_2 in the shallow aquifer (Figure 1). Therefore, it
549 undergoes a degassing process rapidly until it stabilizes at the shallow aquifer conditions of P, T, and
550 CO_2-density. Then, the remaining mass (i.e. dissolved phases) undergoes a mixing process as the plume
551 moves through the porous medium with the local groundwater toward the observation wells (Figure 1) (Ju
552 et al., 2019).

553 From a monitoring point of view, the concentrations of the noble gases will start to deviate
554 gradually from the composition of the air saturated water (ASW) (i.e. green diamond) as the plume
555 approaches an observation point and, at some point, they will vary over the threshold (i.e., the. 3σ line),
556 confirming CO_2 leakage occurrence (Figure 8). Information about the first detection points (i.e., the
557 minimum mixing proportion of the CO_2 plume needed to override the detection limit and the composition

of the noble gas tracer at this point) is listed in Table 2. For example, we can see the first arrival of ^{4}He when the CO_2 plume (1.14%) approaches a monitoring well, which initially loses a CO_2 mass of 1.8×10^{-5} CO_2 cm^3 STP/g H_2O during the degassing event.

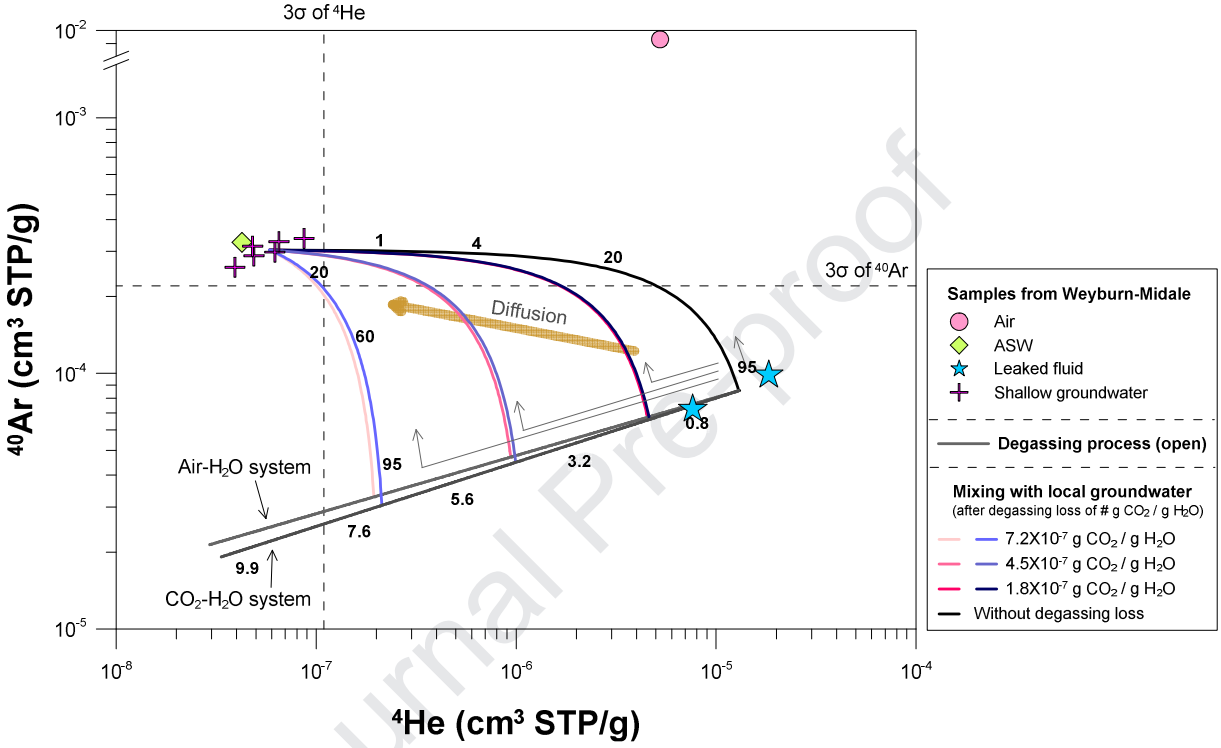

Figure 8. Evolution of a CO_2 plume under physical processes in terms of noble gas concentration. All the measured data and hypothetical values (i.e. leaked fluid) were from Gilfillan et al. (2017). In this scenario, the initial plume is unstable and, therefore, undergoes the degassing process rapidly until stabilization is achieved in the shallow groundwater system (i.e., gray lines). Then, the degassed plume undergoes a dilution process by mixing with local groundwater (i.e., blue or pink lines). Due to the diffusion process, the points can deviate from the degassing-mixing trend and converge toward a natural background level as diluted (i.e., brown arrow), and action of this process can be prominent at the plume boundary or water table as facing a concentration gradient. From a monitoring point of view, the observed concentration will gradually evolve from the Air Saturated Water level (ASW; i.e. green diamond; see Table 1) as the CO_2

plume approaches a monitoring point, and one can eventually notice the CO_2 leakage occurrence when signals override the detection threshold, 3σ value. Note that the degassing process was depicted in both the air–H_2O system and CO_2–H_2O system (see the text for the definition of both systems). The theoretical air–H_2O system is gradually getting apart from the real CO_2–H_2O system, as degassed mass increases (see the gray lines).

In most cases, the ^4He species and their various combinations with other species showed high monitoring efficiencies than the other heavier species, which was attributed to the large amount of ^4He in the CO_2 plume. However, it should be noted that the efficiency of one tracer is fairly dependent on the action of the physical processes in plume migration. For example, if the CO_2 plume lost more than 7.2×10^{-5} CO_2 cm^3 STP/g H_2O during the degassing process, then ^{36}Ar and ^{40}Ar will be ahead of ^4He in the monitoring well (Figure 8). Furthermore, if the diffusion process is dominant at the plume front, ^4He can be delayed behind other heavier species in the monitoring system because of its fast dilution along the concentration gradient, which has been demonstrated in other artificial injection tests (Carrigan et al., 1996; Sanford et al., 1996). Therefore, the detection efficiency in terms of its role as an early warning for CO_2 leakage is dependent only on the leakage conditions, and it cannot be said that any single tracer is superior to others.

4.1.2.2 Influence of density of CO_2 on the monitoring efficiency

Free-phase CO_2 forms a CO_2-rich plume in a shallow aquifer after a leakage event. The partitioning behavior of noble gas is different in pure water and in CO_2-rich plume owing to an increase in the molecular interactions inside a plume with a high CO_2 density (Warr et al., 2015). Until now, the air–H_2O partitioning coefficient has been adopted for describing the distribution of noble gas tracers in a CO-rich system instead of the CO_2–H_2O partitioning coefficient, owing to an absence of previous studies (Gilfillan et al., 2008; LaForce et al. 2014; Zhang et al. 2011). This situation caused uncertainty and errors

in quantitative calculations. For example, Zhou et al. (2012) could not determine a clear reason for mismatches of heavier noble gases to the analytical model, i.e., whether it was caused by the absence of a proper coefficient (i.e., the CO_2–H_2O partitioning coefficient) or by the influence of another physical process (i.e., sedimentary excess Kr; see Figure 12 in that paper). Then, Warr et al. (2015) pointed out the problem; specifically, the partitioning behavior of a noble gas tracer in a CO_2-rich system differs remarkably from that in an air-H_2O water system.

Under CO_2 saturation conditions, i.e., 3.97 kg/m^3 (see Table A.1), the partitioning ratio of ^{4}He species to CO_2 water increased by 2.26%, but those of others decreased, e.g., by up to -7.32% for ^{40}Ar and -23.05% for ^{84}Kr (Table 3). Figure 9 shows the percent change in noble gas concentration with a solubility-controlled process both in an air-H_2O system (pink-colored) and in a CO_2-H_2O system (blue-colored). The CO_2-rich plume will have a lower amount of heavier isotopes compared with that in the air-H_2O system, owing to the difference in water/gas partitioning coefficients between an air-H_2O system and CO_2- H_2O system (see the definition of δ partitioning in Table 3). This trend may affect the quantitative evaluation of the fate of CO_2 (Table 3). However, this effect looks relatively minor in this specific case, owing to the wide distribution of initial values (i.e., blue stars), which cancels out this trend (Figure 8).

Table 3 Percent differences between water/gas partitioning coefficients of noble gases (top) and percent differences between noble gas concentrations in a CO_2–H_2O system and an air–H_2O system (below). The latter was calculated for various degassing events.

	^{4}He	^{40}Ar	^{84}Kr
δpartitioning[†]	---------- %[†] ----------		
	2.26	-7.32	-23.05
Degassing amount[‡]	---------- %[¶] ----------		
0	0	0	0
1.8	2.83	-2.09	-3.94

4.5	7.21	-5.15	-9.57
7.2	11.79	-8.12	-14.86

612 †percent difference of water/gas partitioning coefficient of noble gases (unit: mM/atm) between the two
613 systems, $(k_{i,CO_2-H_2O} - k_{i,air-H_2O})/k_{i,air-H_2O} \times 100$. Partitioning coefficients can be found in Table
614 A.1 of Appendix A.

615 ‡total degassed mass in an open system (unit: $\times 10^{-7}$ cm^3 STP/g).

616 ¶percent difference of concentration (unit: cm^3 STP/g) between the two systems, $(C_{i,CO_2-H_2O} -$
617 $C_{i,air-H_2O})/C_{i,air-H_2O} \times 100$.

618

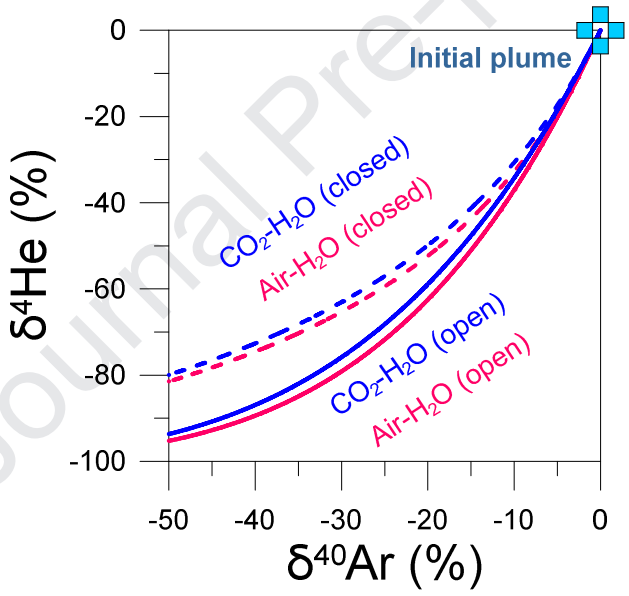

619

620 **Figure 9**. Percent change in noble gas concentration from its initial composition in a CO_2 plume
621 undergoing a degassing process for both air–H_2O and CO_2–H_2O systems. The air–H_2O system was
622 depicted using partitioning coefficients from the NIST chemistry webbook of Sander (2017) (pink-
623 colored), and the CO_2–H_2O system was based on coefficients from Warr et al. (2015) (blue) assuming a
624 CO_2-saturated state (i.e., 3.97 CO_2 kg/m3) at a temperature of 14.3°C, altitude of 580 m, and water
625 column of 10 m (Table A.1). The theoretical air–H_2O system will deviate from the real CO_2–H_2O system

because molecular interactions increase with CO_2 concentration. Note that the difference between the air–H_2O (pink) and CO_2–H_2O (blue-colored) systems is smaller than the difference between the closed (dotted) and open (line) systems (see the text for definition of each system). The noble gas composition of the initial plume was from Gilfillan et al. (2017).

4.1.2.3 Optimal tracers for detecting CO_2 leakage

Although the ^4He tracer appears efficient in tracing the CO_2 leakage owing to its large compositional difference between the two reservoirs (Table 2), the wide variation in ascending CO_2 possibly hinders the accurate quantitative estimation. At the Weyburn site, the variation in ^4He distribution was 58.2% (1σ) for CO_2 (Table 1), and this was attributed to the interaction between CO_2 and crustal fluids that reside in the deep reservoir (Gilfillan et al., 2017). The scattered distribution of initial values can add errors and uncertainty to the evaluation and tracing of the fate of CO_2 (Wilkinson et al., 2010). This issue can be resolved by using atmospheric noble gases such as ^{20}Ne, ^{36}Ar, and ^{84}Kr, which have been adopted as they ignore wide variations due to interactions with reservoir fluids (Ma et al., 2009).

In Figure 10, an anomaly of atmospheric noble gas is depicted with the various physical processes, where clear separation between the mixing (i.e., the light gray zone) and degassing processes (i.e., the dark gray zone) implies the applicability of the tracers to constraining the physical processes. However, when they are plotted together in Figure 11 to explain the evolution of the CO_2 plume, the anomalies driven by the two processes (i.e., mixing and degassing) overlap each other within analytical error ranges and therefore one cannot differentiate one from the other. Moreover, the wide scatters of the initial values (i.e. blue stars) significantly overrode the post-anomaly of the tracers, which was contrary to the results obtained in the case where ^4He is combined with other components (see Figure 8, relative to Figure 11). Other combinations of atmospheric elements also exhibited similar problems, as illustrated in

Supplementary Figure 1. Though atmospheric components have been demonstrated to distinguish physical processes in many studies and have proved useful (Ballentine et al., 1991; Battani et al., 2000; Ma et al., 2009; Zhou et al., 2012), in this particular case, they cannot be used to determine the physical anomalies (Figure 11 and Supplementary Figure 1). This simulation indicated that ^{4}He and its combinations with heavier species are the most powerful proxies for understanding the fate of a CO_2 plume, as they have more distinguishable compositional changes under physical interactions than other combinations. The overall result suggests that it is mandatory to check whether the post-anomaly of a selected tracer (i.e. degassing-mixing trend) cancels out the heterogeneous distribution of reservoir gases.

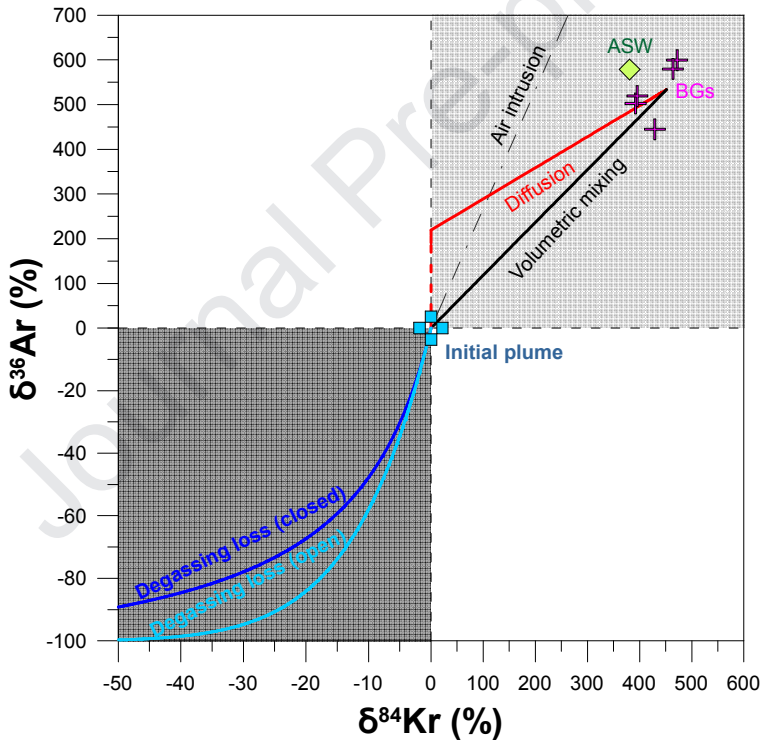

Figure 10. Percent change in noble gas composition in the initial CO_2 plume under various physical processes. BGs (i.e., pink cross symbols) present the concentrations of shallow aquifer samples, and ASW is the air saturated water in a local groundwater condition (i.e., green diamond; see Table 1). Note that the

distinction between mixing processes (i.e. the light gray zone) and solubility-controlled processes (i.e. the dark gray zone) is apparent. All the measured data were from Gilfillan et al. (2017).

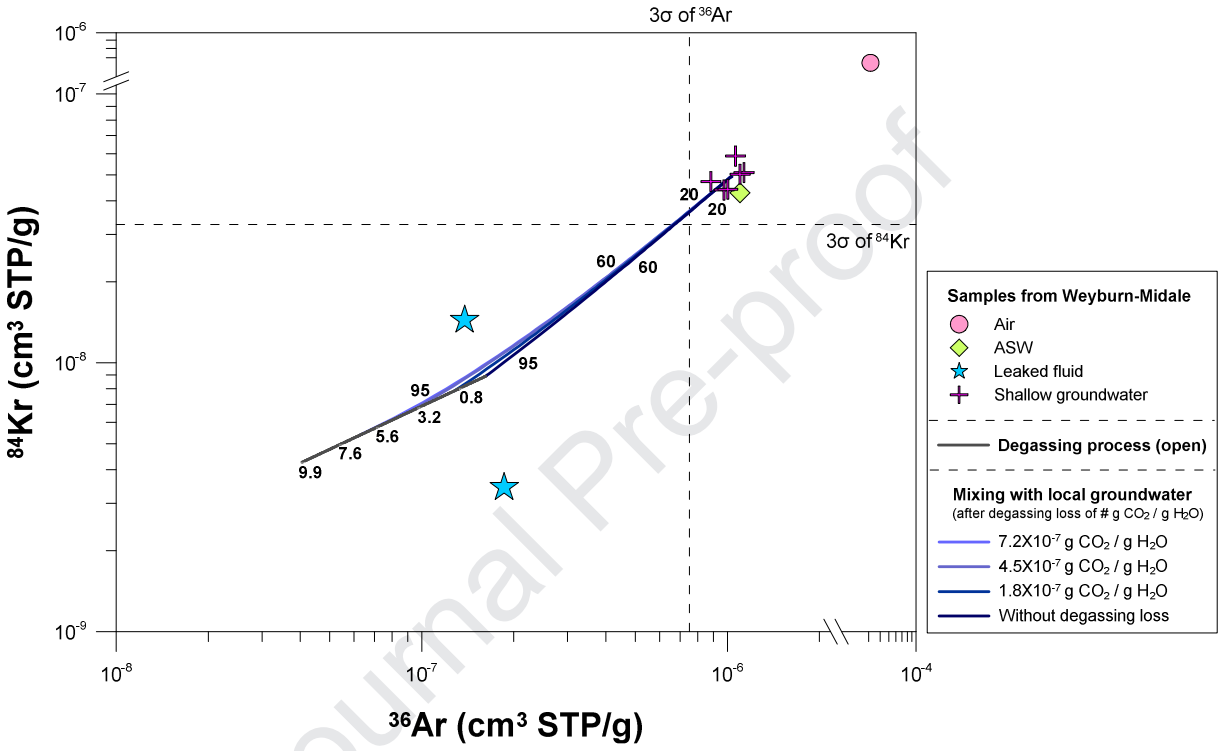

Figure 11. Evolution of a CO_2 plume under physical processes in terms of atmospheric noble gas concentration. All the measured data were from Gilfillan et al. (2017). In this scenario, the initial plume is unstable and, therefore, undergoes a degassing process rapidly until stabilization in a shallow groundwater system is achieved (i.e., the gray line) (see Figure 1). Then, the degassed plume undergoes a dilution process when it mixes with local groundwater (i.e., the blue lines). Note that the degassing and mixing process overlap each other and cannot be separated from the other. Furthermore, see that the wide distribution of the initial values (i.e., blue stars) cancels out the post anomaly.

4.2 Identifying leakage hot spots using noble gas fingerprint in an actual CO_2 leakage site

673 Accidental leakage from a deep reservoir into a shallow system can happen through various
674 pathways, such as an injection well, an abandoned well, or natural conduits (e.g., faults or poor caprock
675 integrity), possibly exposing CO_2 at various points in shallower groundwater. This suggests that the actual
676 CO_2 leakage we would observe in a shallow aquifer is complicated and cannot be easily discussed with a
677 noble gas fingerprint.

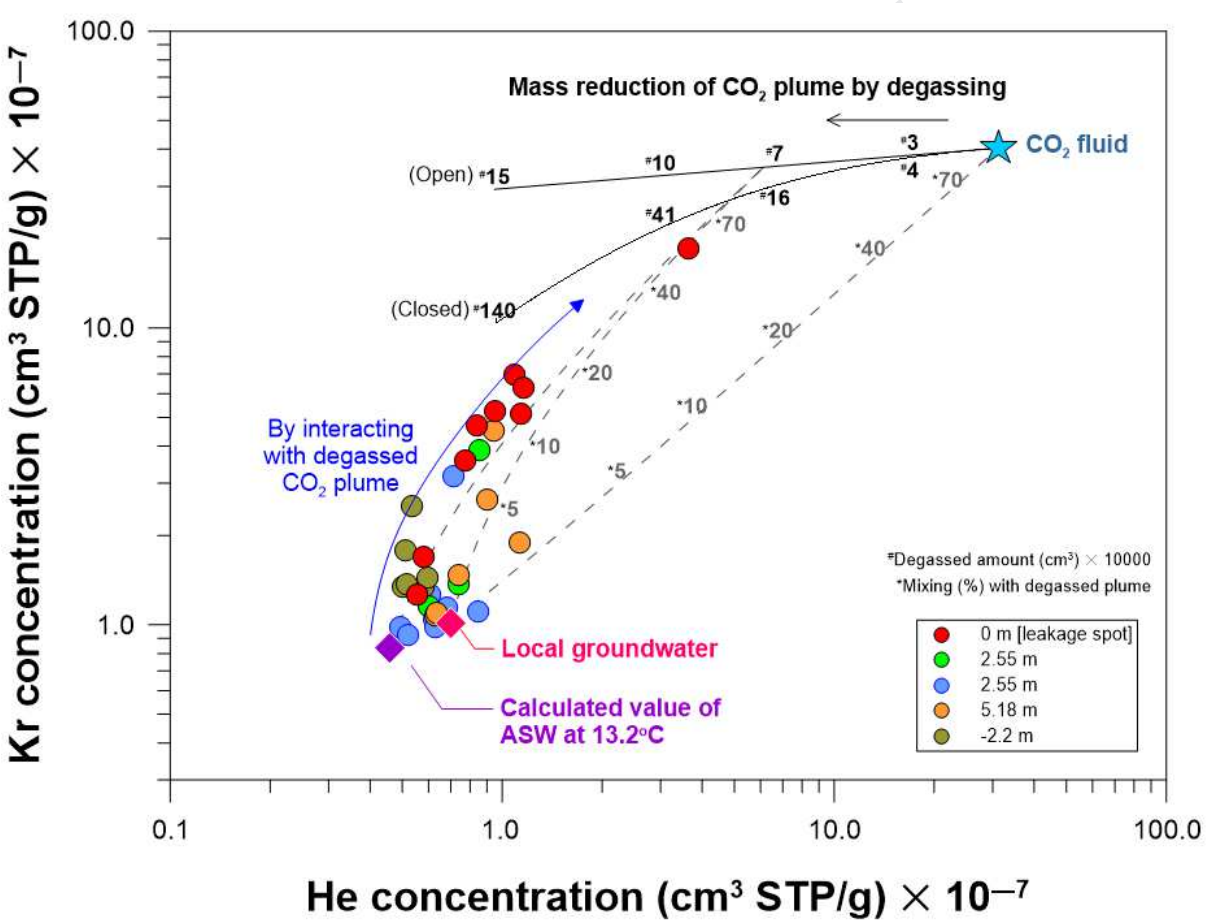

678

679 **Figure 12**. He–Kr plot after CO_2 leakage into a shallow groundwater is allowed to occur; the plot was
680 modified form Ju et al. (2019). The samples were lying on the new dilution line of the mixing trajectory
681 between a partially degassed CO_2 plume and a background concentration (i.e. the pink/purple diamond).
682 In other words, the samples were a mixture of the degassed CO_2 plume and the local groundwater. Note

683 that the leakage spot (0 m; i.e., red circles) exhibited the largest variation in the mixing trajectory as the
684 CO_2 plume interacted with the degassed CO_2 plume. The other samples were collected at a certain
685 distance from the leakage point, and they exhibited a smaller variation.

686 The actual CO_2 leakage can complicate the noble gas distribution as ascending CO_2 takes various
687 paths into a shallow aquifer. However, we can still trace the CO_2 leakage by systematic and scientific
688 investigation. In the environmental forensic world, when attempting to trace a source spot in close
689 proximity, one can make use of an evolutionary pattern of a source compound (Morrison, 1999).
690 Similarly, from the artificial injection tests, we also observed an evolutionary path of a leaked plume
691 where the noble gas composition undergoes a series of modification steps owing to physical processes (i.e.
692 degassing-mixing trend in Figure 8). This specific trend also has been shown in the artificial CO_2
693 injection test in a shallow aquifer (Ju et al., 2019) and natural CO_2 production site (Zhou et al., 2005).

694 In terms of the evolutionary path, another representative result was demonstrated in Figure 12
695 following an artificial injection of CO_2 into shallow aquifer (Ju et al., 2019) In Figure 12, the monitoring
696 data is plotted on the gradual trend between the degassing-end (i.e. the intercept between black line and
697 dotted line) and the local groundwater (i.e. diamond symbols) (Ju et al., 2019). The trend indicated that
698 the degassed plume was gradually mixed with local groundwater after the solubility-controlled process
699 was swiftly finished. Here, the samples from a leakage spot (i.e., the red circles) exhibit the widest
700 variation on the mixing line, which stretches from the degassing-end. This was attributed to the
701 monitoring well, which was located at the closest point to a leakage spot and therefore efficiently
702 captured the CO_2 plume shortly after the degassing-end. There is a clear distinction between the source
703 spot (i.e. wide variation) and the other monitoring wells besides the leakage spot (i.e. narrow variation
704 around the local BG), suggesting that, with this trend, a leaking point with an actual CO_2 leakage event
705 can potentially be identified. Therefore, the evolutionary path of the leaked plume elucidated in this study
706 can be an important fingerprint when monitoring CO_2 leakage using a noble gas tracer.

5 Conclusions

Although noble gas tracers have been proven useful in characterizing the fate of CO_2 in many aspects of CO_2 storage research, they have not been extensively used for monitoring CO_2, i.e., to trace leaked CO_2 in shallow groundwater. Furthermore, noble gas application has been limited to the monitoring of natural analogue sites and CCS pilot test sites, suggesting we still need to link previous findings to an actual CO_2 leakage event. Therefore, this study evaluated the applicability of noble gas tracers to monitoring actual CO_2 leakage from a deep reservoir into a shallow groundwater system.

First, an artificial injection test was performed in a shallow-depth aquifer system to observe and verify observations from previous researches. Here, we used inert gas tracers (i.e., SF_6 and noble gases) to separate and explain the physical interactions that determine the fate of the leaked plume. During the tests, the fate of the leaked plume was a function of a solubility-controlled process (i.e., degassing) and a mixing process. This result was consistent with those of Ju et al. (2019) and Zhou et al. (2005), suggesting that the two processes are primarily responsible for the fate of the leaked plume in a shallow system.

While the artificial injection tests identified the major interactions responsible for the fate of the leaked plume, the applicability of tracers to actual leakage monitoring work at a CCS site has not been explored. Therefore, repeated simulations were conducted based on data from a real CO_2 injection site (the Weyburn and Midale oil fields) to predict the fate and evolutionary path of a leaked plume that we would observe with actual CO_2 leakage. This simulation indicated that ^4He and its combinations with heavier species are useful monitoring parameters for evaluating the fate of a leaked plume. In contrast, in terms of early warning of a leakage, none of the tracers were superior to the others, as their detection efficiencies appear to be dependent on the leakage conditions and therefore under the control of physical processes. Furthermore, the high density of the CO_2 of a leaked plume possibly adds uncertainty and

errors to the quantitative evaluations. However, the wide scatter of the initial values (i.e., noble gas variation in produced CO_2) significantly overrides the effect of the other uncertainties in monitoring CO_2 leakage at this specific site. This suggests the homogeneity of the initial plume is significantly important in terms of the monitoring efficiency using noble gas tracers. Overall, the results of this study revealed that a noble gas can be applied not only for qualitative purposes (i.e., leaking detection), but also for identifying mass allocations and the evolutionary path of a leaked plume in a shallow aquifer system. Most importantly, the leaked plume has a unique evolutionary path in terms of noble gas tracers, which are expected to act as important fingerprints for tracing a leakage spot as complex mechanisms affect the CO_2 plume distribution.

Acknowledgements

This research was supported by a Korea Environmental Industry & Technology Institute (KEITI) grant entitled “R&D Project on Environmental Management of Geologic CO2 Storage” (Project Number: 2018001810002), by a Korea Polar Research Institute grant (PE19060) and by a National Research Foundation of Korea (NRF) grant funded by the Korean government (MSIT) (No. 0409-20190119). We thank all the members of the K-COSEM team and, appreciate Intae Kim and Minjung Kim for their efforts and support on noble gas analysis.

Appendix A. Analytical solutions for the fate of CO_2 plume

When degassing happens in a closed system, the exsolved gas will still remain in the aquifer system, and an equilibrium will be achieved at the interfaces between the bubbles and remaining plume. In this situation, one-step partitioning determines the noble gas distribution, which is defined by Henry's constant, such as in Eq.(A.1) and Eq. (A.2) (Ballentine et al., 2002):

$$(\frac{A}{B})_{(g)} = (\frac{A}{B})_{(l)} \times \alpha \quad \text{Eq. (A. 1)}$$

$$\alpha = \frac{\frac{r_A}{\emptyset_A}K_A}{\frac{r_B}{\emptyset_B}K_B} \quad \text{Eq. (A. 2)}$$

Here:

$(\frac{A}{B})_{(g)}$ = A and B ratio in exsolved bubbles, where A and B are different noble gases;

$(\frac{A}{B})_{(l)}$ = the composition of A and B remaining in the dissolved phase;

α = partitioning coefficient for gas/liquid system;

K_A, K_B = Henry's constant for A and B (Table A.1);

Table A.1 Partitioning coefficients of noble gas tracers in pure water and CO_2 saturated water.

	He	Ne	Ar	Kr
	mM/atm			
Pure water[†]	0.389	0.482	1.711	3.211
CO_2 saturated water[‡]	0.398	-	1.586	2.471

[†]NIST chemistry webbook of Sander (2017) at temperature of 14.3°C.

[‡]calculated according to Warr et al. (2015) where CO_2 saturated water (3.97 kg/m^3) was assumed in temperature of 14.3°C, altitude of 580 m and water column of 10 m.

764 r_A, r_B = dissolved phase activity coefficients for A and B; and

765 $\emptyset_A$, $\emptyset_B$ = gas phase fugacity coefficients for A and B.

766 A Rayleigh equation was used to explain the degassing procedure in the open system, where gas
767 bubbles continuously strip off the dissolved noble gas from the aquifer system at the gas/liquid interfaces
768 of the exsolved bubbles until the end of the process (Ballentine et al., 2002; Zhou et al., 2005; Holland
769 and Gilfillan, 2013).

770 $$(\frac{A}{B})_{(l)} = (\frac{A}{B})_0 \times f^{\alpha-1} \quad \text{Eq. (A. 3)}$$

771 $(\frac{A}{B})_{(l)}$ = The composition of A and B remaining in the aquifer

772 $(\frac{A}{B})_{(0)}$ = The composition of A and B in initial CO_2 plume

773 f = Fraction of element B remaining in dissolved plume

774 The plume is diluted by the diffusion process in the aquifer system, along the concentration
775 gradient between the plume and local groundwater. In dominance of this process, the distribution of noble
776 gas element is defined by the diffusion coefficient and the elapsed time since the leakage event happened,
777 such as in Eq. (A. 4) (Fetter, 1999):

778 $$C = \frac{(C_0 - C_i)V}{(4\pi t)^{3/2}\sqrt{D_x D_y D_z}} \quad \text{Eq. (A. 4)}$$

779 Here:

780 C = maximum concentration of element in leaked plume at a specific time, t (cm^3 STP/g);

781 C_0 = initial concentration of element in the leaked plume (cm^3 STP/g);

782 C_i = concentration of element in aquifer before leakage (cm^3 STP/g);

783 V = volume of the initial leaked plume (cm^3);

784 t = elapsed time since leakage (s); and

785 D_x, D_y, D_z = diffusion coefficients of element for x, y, z direction, respectively (cm^2/s) (Table A.2).

786 **Table A.2** Diffusion coefficients of noble gas tracers in water

	He	Ne	Ar‡	Kr
	cm^2/s			
Pure Water†	6.12×10^{-5}	3.23×10^{-5}	1.94×10^{-5}	1.36×10^{-5}

787 †Jähne et al. (1987) at temperature of 14.3°C.

788 ‡Wise and Houghton (1966) at temperature of 14.3°C.

References

Alcalde, J., Flude, S., Wilkinson, M., Johnson, G., Edlmann, K., Bond, C.E., Scott, V., Gilfillan, S.M.V., Ogaya, X., Haszeldine, R.S., 2018. Estimating geological CO_2 storage security to deliver on climate mitigation. Nat. Commun. 9(1), 2201. https://doi.org/10.1038/s41467-018-04423-1.

Altman, S.J., Aminzadeh, B., Balhoff, M.T., Bennett, P.C., Bryant, S.L., Cardenas, M.B., DiCarlo, D.A., Eichhubl, P., Hesse, M.A., Huh, C., Matteo, E.N., Mehmani, Y., Tenney, C.M., Yoon, H.J., 2014. Chemical and hydrodynamic mechanisms for long-term geological carbon storage. J. Phys. Chem. C. 118(28), 15103–15113. https://doi.org/10.1021/jp5006764.

Baek, W., Lee, J.Y., 2011. Source apportionment of trichloroethylene in groundwater of the industrial complex in Wonju, Korea: a 15□year dispute and perspective. Water Environ. J. 25(3), 336–344. https://doi.org/10.1111/j.1747-6593.2010.00226.x.

Ballentine, C.J., O'nions, R.K., Oxburgh, E.R., Horvath, F., Deak, J., 1991. Rare gas constraints on hydrocarbon accumulation, crustal degassing and groundwater flow in the Pannonian Basin. Earth Planet Sci. Lett. 105(1–3), 229–246. https://doi.org/10.1016/0012-821X(91)90133-3.

Ballentine, C.J., O'nions, R.K., 1994. The use of natural He, Ne and Ar isotopes to study hydrocarbon-related fluid provenance, migration and mass balance in sedimentary basins. Geological Society, London, Special Publications 78(1), 347–361. https://doi.org/10.1144/GSL.SP.1994.078.01.23.

Ballentine, C.J., Burgess, R., Marty, B., 2002. Tracing Fluid Origin, Transport and Interaction in the Crust, In: Porcelli, D., Ballentine, C.J., Wieler, R. (Eds.), Reviews in Mineralogy & Geochemistry Volume 47, Noble Gases in Geochemistry and Cosmochemistry, pp. 539–614.

809 Battani, A., Sarda, P., Prinzhofer, A., 2000. Basin scale natural gas source, migration and trapping traced
810 by noble gases and major elements: the Pakistan Indus basin. Earth Planet Sci. Lett. 181(1-2), 229–249.
811 https://doi.org/10.1016/S0012-821X(00)00188-6.

812 Beaubien, S.E., Jones, D.G., Gal, F., Barkwith, A.K.A.P., Braibant, G., Baubron, J.C., Ciotoli, G.,
813 Graziani, S., Lister, T.R., Lombardi, S., Michel, K., Quattrocchi, F., Michel, K., 2013. Monitoring of
814 near-surface gas geochemistry at the Weyburn, Canada, CO_2-EOR site, 2001–2011. Int. J. Greenh. Gas
815 Control 16, 236–262. https://doi.org/10.1016/j.ijggc.2013.01.013.

816 Beyerle, U., Aeschbach-Hertig, W., Imboden, D.M., Baur, H., Graf, T., Kipfer, R., 2000. A mass
817 spectrometric system for the analysis of noble gases and tritium from water samples. Environ. Sci.
818 Technol. 34(10), 2042–2050. https://doi.org/10.1021/es990840h.

819 Bosch, A., Mazor, E., 1988. Natural gas association with water and oil as depicted by atmospheric noble
820 gases: case studies from the southeastern Mediterranean Coastal Plain. Earth Planet Sci. Lett. 87(3),
821 338–346. https://doi.org/10.1016/0012-821X(88)90021-0.

822 Carrigan, C.R., Heinle, R.A., Hudson, G.B., Nitao, J.J., Zucca, J.J., 1996. Trace gas emissions on
823 geological faults as indicators of underground nuclear testing. Nature 382(6591), 528–531.

824 Chen, M., Park, M., Kim, J.H., Shinn, Y.J., Lee, Y.K., Hur, J., 2018. Exploring pore water
825 biogeochemical characteristics as environmental monitoring proxies for a CO_2 storage project in
826 Pohang Basin, South Korea. Mar. Pollut. Bull. 137, 331–338.
827 https://doi.org/10.1016/j.marpolbul.2018.10.036.

828 Cohen, G., Loisy, C., Laveuf, C., Le Roux, O., Delaplace, P., Magnier, C., Rouchon, V., Garcia, B.,
829 Cerepi, A., 2013. The CO_2-Vadose project: Experimental study and modelling of CO_2 induced leakage

and tracers associated in the carbonate vadose zone. Int. J. Greenh. Gas Control 14, 128–140. https://doi.org/10.1016/j.ijggc.2013.01.008.

Fanale, F.P., Cannon, W.A., 1971. Physical adsorption of rare gases on terrigenous sediments. Earth Planet Sci. Lett. 11, 362–368.

Fetter, C.W., 1999. Contaminant hydrogeology, 2nd edn. Prentice-Hall, New York, pp. 70–74.

Flude, S., Johnson, G., Gilfillan, S.M., Haszeldine, R.S., 2016. Inherent tracers for carbon capture and storage in sedimentary formations: composition and applications. Environ. Sci. Technol. 50(15), 7939–7955. https://doi.org/10.1021/acs.est.6b01548.

Gilfillan, S.M.V., Ballentine, C.J., Holland, G., Blagburn, D., Sherwood Lollar, B., Scott, S., Schoell, M., Cassidy, M., 2008. The noble gas geochemistry of natural CO_2 gas reservoirs from the Colorado Plateau and Rocky Mountain provinces, USA. Geochim. Cosmochim. Acta 72, 1174–1198. https://doi.org/10.1016/j.gca.2007.10.009.

Gilfillan, S.M.V, Lollar, B.S., Holland, G., Blagburn, D., Stevens, S., Schoell, M., Cassidy, M., Ding, Z., Zhou, Z., Lacrampe-Couloume, G., Ballentine, C.J., 2009. Solubility trapping in formation water as dominant CO_2 sink in natural gas fields. Nature 458(7238), 614–618. https://doi.org/10.1016/j.gca.2007.10.009.

Gilfillan, S.M.V, Wilkinson, M., Haszeldine, R.S., Shipton, Z.K., Nelson, S.T., Poreda, R.J., 2011. He and Ne as tracers of natural CO_2 migration up a fault from a deep reservoir. Int. J. Greenh. Gas Control 5(6), 1507–1516. https://doi.org/10.1016/j.ijggc.2011.08.008.

Gilfillan, S.M.V, Sherk, G.W., Poreda, R.J., Haszeldine, R.S., 2017. Using noble gas fingerprints at the Kerr Farm to assess CO_2 leakage allegations linked to the Weyburn-Midale CO_2 monitoring and storage project. Int. J. Greenh. Gas Control 63, 215–225. https://doi.org/10.1016/j.ijggc.2017.05.015.

852 Györe, D., Stuart, F.M., Gilfillan, S.M.V., Waldron, S., 2015. Tracing injected CO_2 in the Cranfield
853 enhanced oil recovery field (MS, USA) using He, Ne and Ar isotopes. Int. J. Greenh. Gas Control 42,
854 554–561. https://doi.org/10.1016/j.ijggc.2015.09.009.

855 Györe, D., Gilfillan, S.M.V., Stuart, F.M., 2017. Tracking the interaction between injected CO_2 and
856 reservoir fluids using noble gas isotopes in an analogue of large-scale carbon capture and storage. Appl.
857 Geochem. 78, 116–128. https://doi.org/10.1016/j.apgeochem.2016.12.012.

858 Györe, D., McKavney, R., Gilfillan, S.M.V., Stuart, F.M., 2018. Fingerprinting coal-derived gases from
859 the UK. Chem. Geol. 480, 75–85. https://doi.org/10.1016/j.chemgeo.2017.09.016.

860 Heilweil, V.M., Solomon, D.K., Perkins, K.S., Ellett, K.M., 2004. Gas□Partitioning Tracer Test to
861 Quantify Trapped Gas During Recharge. Groundwater 42(4), 589–600. https://doi.org/10.1111/j.1745-
862 6584.2004.tb02627.x.

863 Holland, G., Gilfillan, S., 2013. Application of noble gases to the viability of CO_2 storage. In: Burnard, P.
864 (Eds.), The Noble Gases as Geochemical Tracers. Advances in Isotope Geochemistry, Springer, Berlin,
865 Heidelberg, pp. 177–223. https://doi.org/10.1007/978-3-642-28836-4_8.

866 IPCC, 2005. IPCC special report on carbon dioxide capture and storage, Metz, B., Davidson, O., de
867 Coninck, H.C., Loos, M., Meyer, L.A. (Eds.), Prepared by Working Group III of the Intergovernmental
868 Panel on Climate Change. Cambridge University Press, Cambridge, United Kingdom/New York, NY,
869 USA, pp. 208–210.

870 Jähne, B., Heinz, G., Dietrich, W., 1987. Measurement of the diffusion coefficients of sparingly soluble
871 gases in water. J. Geophys. Res.: Oceans 92(C10), 10767–10776.
872 https://doi.org/10.1029/JC092iC10p10767.

873 Ju, Y., Beaubien, S.E., Lee, S.S., Kaown, D., Hahm, D., Lee, S., Park, I.W., Park, K., Yun, S.T., Lee,
874 K.K., 2019. Application of natural and artificial tracers to constrain CO_2 leakage and degassing in the
875 K-COSEM site, South Korea. Int. J. of Greenh. Gas Control 86, 211–225.
876 https://doi.org/10.1016/j.ijggc.2019.05.002.

877 Ju, Y., Lee, S.S., Kaown, D., Lee, K.K., 2018. Application of Inert Gas Tracers to Identify the Physical
878 Processes Governing the Mass Balance Problem of Leaking CO_2 in Shallow Groundwater System. 14th
879 Greenhouse Gas Control Technologies Conference; Melbourne; Australia; October 21–26.
880 https://papers.ssrn.com/sol3/papers.cfm?abstract_id=3365686.

881 Ju, Y., Kaown, D., Lee, K.K., 2018. A three-pronged approach for identifying source and extent of nitrate
882 contamination in groundwater. J. Soil Water Conserv. 73(5), 493–503.
883 https://doi.org/10.2489/jswc.73.5.493.

884 Jung, N.H., Han, W.S., Han, K., Park, E., 2015. Regional□scale advective, diffusive, and eruptive
885 dynamics of CO_2 and brine leakage through faults and wellbores. J. Geophys. Res. Solid Earth 120(5),
886 3003–3025. https://doi.org/10.1002/2014JB011722.

887 Kaown, D., Shouakar□Stash, O., Yang, J., Hyun, Y., Lee, K.K., 2014. Identification of multiple sources
888 of groundwater contamination by dual isotopes. Groundwater 52(6), 875–885.
889 https://doi.org/10.1111/gwat.12130.

890 Kilgallon, R., Gilfillan, S.M.V., Edlmann, K., McDermott, C.I., Naylor, M., Haszeldine, R.S., 2018.
891 Experimental determination of noble gases and SF_6, as tracers of CO_2 flow through porous sandstone.
892 Chem. Geol. 480, 93–104. https://doi.org/10.1016/j.chemgeo.2017.09.022.

Kim, H.H., Lee, S.S., Ha, S.W., Lee, K.K., 2018. Application of single-well push-drift-pull tests using dual tracers (SF_6 and salt) for designing CO_2 leakage monitoring network at the Environmental Impact Test site in Korea. Geosci. J. 22(6), 1041–1052. https://doi.org/10.1007/s12303-018-0045-9.

Kim, H.H., Koh, E.H., Lee, S.S., Lee, K.K., 2019. Biased Estimation of Groundwater Velocity from a Push-Pull Tracer Test Due to Plume Density and Pumping Rate. Water 11(8), 1558. https://doi.org/10.3390/w11081558.

Koo, C.M., Lee, K., Kim, M., Kim, D.O., 2005. Automated system for fast and accurate analysis of SF_6 injected in the surface ocean. Environ. Sci. Technol. 39(21), 8427–8433. https://doi.org/10.1021/es050149g.

LaForce, T., Ennis-King, J., Boreham, C., Paterson, L., 2014. Residual CO_2 saturation estimate using noble gas tracers in a single-well field test: the CO2CRC Otway project. Int. J. Greenh. Gas Control 26, 9–21. https://doi.org/10.1016/j.ijggc.2014.04.009.

Lee, K.K., Ellsworth, W.L., Giardini, D., Townend, J., Ge, S., Shimamoto, T., Yeo, I.W., Kang, T.S., Rhie, J., Sheen, D.H., Chang, C., Woo, J.U., Langenbruch, C., 2019. Managing injection-induced seismic risks. Science, 364(6442), 730–732. https://doi.org/10.1126/science.aax1878.

Lee, K.K., Lee, S.H., Yun, S.T., Jeen, S.W., 2016. Shallow groundwater system monitoring on controlled CO_2 release sites: a review on field experimental methods and efforts for CO_2 leakage detection. Geosci. J. 20(4), 569–583. https://doi.org/10.1007/s12303-015-0060-z.

Lee, S.S., Ju, Y., HA, S.W., Joun, W.T., Jun, S.C., Yun, S.T., Lee, K.K., 2018. Controlled CO_2 Injection into a Shallow Aquifer and Leakage Detection Monitoring by Two Different Leakage Events at the K-Cosem Site, Korea. In 14th Greenhouse Gas Control Technologies Conference Melbourne; Australia; October 21–26. https://papers.ssrn.com/sol3/papers.cfm?abstract_id=3366360.

915 Lee, S.S., Kim, H.H., Joun, W.T., Lee, K.K., 2017. Design and Construction of Groundwater Monitoring
916 Network at Shallow-depth CO_2 Injection and Leak Test Site, Korea. Energy Procedia 114, 3060–3069.
917 https://doi.org/10.1016/j.egypro.2017.03.1434.

918 Lollar, B.S., Ballentine, C.J., Onions, R.K., 1997. The fate of mantle-derived carbon in a continental
919 sedimentary basin: integration of C/He relationships and stable isotope signatures. Geochim.
920 Cosmochim. Acta 61(11), 2295–2307. https://doi.org/10.1016/S0016-7037(97)00083-5.

921 Lott, D.E., Jenkins, W.J., 1998. Advances in analysis and shipboard processing of tritium and helium
922 samples. International WOCE Newsletter 30, 27–30.

923 Lu, J., Cook, P.J., Hosseini, S.A., Yang, C., Romanak, K.D., Zhang, T., Freifeld, B.M., Smyth, R.C.,
924 Zeng, H., Hovorka, S.D., 2012. Complex fluid flow revealed by monitoring CO_2 injection in a fluvial
925 formation. J. Geophys. Res. Solid Earth 117, B03208. https://doi.org/10.1029/2011JB008939.

926 Ma, L., Castro, M.C., Hall, C.M., 2009. Atmospheric noble gas signatures in deep Michigan Basin brines
927 as indicators of a past thermal event. Earth Planet Sci. Lett. 277(1–2), 137–147.
928 https://doi.org/10.1016/j.epsl.2008.10.015.

929 Morrison, R.D., 1999. Environmental forensics: principles and applications. CRC, Boca Raton, FL, pp.
930 209–242.

931 Myers, M., Stalker, L., Pejcic, B., Ross, A., 2013. Tracers–Past, present and future applications in CO_2
932 geosequestration. Appl. Geochem. 30, 125–135. https://doi.org/10.1016/j.apgeochem.2012.06.001.

933 Pinti, D.L., Marty, B., 1995. Noble gases in crude oils from the Paris Basin, France: Implications for the
934 origin of fluids and constraints on oil-water-gas interactions. Geochim. Cosmochim. Acta 59(16),
935 3389–3404. https://doi.org/10.1016/0016-7037(95)00213-J.

936 Podosek, F.A., Bernatowicz, T.J., Kramer, F.E., 1981. Adsorption of xenon and krypton on shales.
937 Geochim. Cosmochim. Acta 45(12), 2401–2415. https://doi.org/10.1016/0016-7037(81)90094-6.

938 Prinzhofer, A., 2013. Noble gases in oil and gas accumulations. In: Burnard, P. (Eds.), Noble Gases as
939 Geochemical Tracers. Springer, New York, pp. 225–247.

940 Rillard, J., Loisy, C., Le Roux, O., Cerepi, A., Garcia, B., Noirez, S., Rouchon, V., Delaplaceb, P.,
941 Willequet, O., Bertrand, C., 2015. The DEMO-CO_2 project: A vadose zone CO_2 and tracer leakage
942 field experiment. Int. J. Greenh. Gas Control 39, 302–317. https://doi.org/10.1016/j.ijggc.2015.04.012.

943 Risk, D., Lavoie, M., Nickerson, N., 2015. Using the Kerr investigations at Weyburn to screen
944 geochemical tracers for near-surface detection and attribution of leakage at CCS/EOR sites. Int. J.
945 Greenh. Gas Control 35, 13–17. https://doi.org/10.1016/j.ijggc.2015.01.019.

946 Sander, R., 2017. Henry's Law Constants. In: Linstrom, P.J., Mallard, W.G. (Eds.), NIST Chemistry
947 WebBook, NIST Standard Reference Database Number 69. National Institute of Standards and
948 Technology, Gaithersburg MD, 20899. https://doi.org/10.18434/T4D303.

949 Sanford, W.E., Shropshire, R.G., Solomon, D.K., 1996. Dissolved gas tracers in groundwater: Simplified
950 injection, sampling, and analysis. Water Resour. Res. 32(6), 1635–1642.
951 https://doi.org/10.1029/96WR00599.

952 Stalker, L., Boreham, C., Underschultz, J., Freifeld, B., Perkins, E., Schacht, U., and Sharma, S., 2015.
953 Application of tracers to measure, monitor and verify breakthrough of sequestered CO_2 at the CO2CRC
954 Otway Project, Victoria, Australia. Chem. Geol. 399, 2–19.
955 https://doi.org/10.1016/j.chemgeo.2014.12.006.

Stanley, R.H., Jenkins, W.J., Lott, D.E., Doney, S.C., 2009. Noble gas constraints on air□sea gas exchange and bubble fluxes. J. Geophys. Res.: Oceans 114(C11), C11020. https://doi.org/10.1029/2009JC005396.

Torgersen, T., Kennedy, B.M., 1999. Air-Xe enrichments in Elk Hills oil field gases: role of water in migration and storage. Earth Planet Sci. Lett. 167(3–4), 239–253. https://doi.org/10.1016/S0012-821X(99)00021-7.

Torgersen, T., Kennedy, B.M., van Soest, M.C., 2004. Diffusive separation of noble gases and noble gas abundance patterns in sedimentary rocks. Earth Planet Sci. Lett. 226(3–4), 477–489. https://doi.org/10.1016/j.epsl.2004.07.030.

Warr, O., Rochelle, C.A., Masters, A., Ballentine, C.J., 2015. Determining noble gas partitioning within a CO_2–H_2O system at elevated temperatures and pressures. Geochim. Cosmochim. Acta 159, 112–125. https://doi.org/10.1016/j.gca.2015.03.003.

Whiticar, M.J., 1999. Carbon and hydrogen isotope systematics of bacterial formation and oxidation of methane. Chem. Geol. 161(1–3), 291–314. https://doi.org/10.1016/S0009-2541(99)00092-3.

Wilkinson, M., Gilfillan, S.M.V., Haszeldine, R.S., Ballentine, C.J., 2010. Plumbing the depths: testing natural tracers of subsurface CO_2 origin and migration, Utah. In: Grobe, M., Pashin, J.C., Dodge, R.L. (Eds.), Carbon Dioxide Sequestration in Geological Media – State of the Science, vol. 59. American Association of Petroleum Geologists Studies, pp. 619-634. https://doi.org/10.1306/13171266St591353.

Wise, D.L., Houghton, G., 1966. The diffusion coefficients of ten slightly soluble gases in water at 10–60^{o}C. Chem. Eng. Sci. 21(11), 999–1010. https://doi.org/10.1016/0009-2509(66)85096-0.

976 Yu, S.Y., Chae, G.T., Jeon, K.H., Jeong, J.S., Park, J.G., 2006. Trichloroethylene contamination in
977 fractured bedrock aquifer in Wonju, South Korea. Bull. Environ. Contam. Toxicol. 76(2), 341–348.
978 https://doi.org/10.1007/s00128-006-0927-9.

979 Zhang, Y., Freifeld, B., Finsterle, S., Leahy, M., Ennis-King, J., Paterson, L., Dance, T., 2011. Single-
980 well experimental design for studying residual trapping of supercritical carbon dioxide. Int. J. Greenh.
981 Gas Control 5(1), 88–98. https://doi.org/10.1016/j.ijggc.2010.06.011.

982 Zhou, Z., Ballentine, C.J., Kipfer, R., Schoell, M., Thibodeaux, S., 2005. Noble gas tracing of
983 groundwater/coalbed methane interaction in the San Juan Basin, USA. Geochim. Cosmochim. Acta
984 69(23), 5413–5428. https://doi.org/10.1016/j.gca.2005.06.027.

985 Zhou, Z., Ballentine, C.J., Schoell, M., Stevens, S.H., 2012. Identifying and quantifying natural CO_2
986 sequestration processes over geological timescales: The Jackson Dome CO2 Deposit, USA. Geochim.
987 Cosmochim. Acta 86, 257–275. https://doi.org/10.1016/j.gca.2012.02.028.

Highlights

- Gas-charged water was injected into an aquifer to demonstrate CO_2 leakage
- Noble gases identified physical processes involved in the fate of gas-charged water
- Based on the injection tests, the fate of leaked CO_2 was studied using noble gases
- The evolutionary path of leaked CO_2 was depicted using noble gases for Weyburn site
- The evolutionary path can act as a fingerprint for identifying a leakage hot spot

Declaration of interests

☒ The authors declare that they have no known competing financial interests or personal relationships that could have appeared to influence the work reported in this paper.

☐The authors declare the following financial interests/personal relationships which may be considered as potential competing interests: